PREDIS

Deliverable 4.9
Leaching behavior of magnesium phosphate cement-based materials

Date 28.6.2024 Version Final

Dissemination level: Public

Vladimir Shkuropatenko,
Sergey Sayenko
Yevhenii Svitlycnyi
KIPT, Ukraine

Laura Diaz Caselles
Céline Cau Dit Coumes*
Angélique Rousselet
CEA France

Email : shkuropatenko@kipt.kharkov.ua; sergeysayenko2@gmail.com; esvitlychniy@i.ua
laura.diazcaselles@cea.fr; celine.cau-dit-coumes@cea.fr; angelique.rousselet@cea.fr

* Corresponding author – celine.cau-dit-coumes@cea.fr

This project has received funding from the Euratom research and training programme 2019-2020 under grant agreement No 945098.

Project acronym PREDIS	Project title PRE-DISposal management of radioactive waste	Grant agreement No. 945098
Deliverable No. D4.9	Deliverable title Leaching behavior of magnesium phosphate cement paste samples	Version Final
Type Report	Dissemination level Public	Due date M46
Lead beneficiary CEA		WP No. 4
Main authors KIPT: Vladimir SHKUROPATENKO, Sergey SAYENKO ; CEA: Laura DIAZ CASELLES, Céline CAU DIT COUMES	Reviewed by Abdesselam ABDELOUAS, IMT, WP4 Leader	Accepted by Maria OKSA, VTT, Coordinator
Contributing author(s) KIPT: Yevhenii SVITLYCNYI ; CEA: Angélique ROUSSELET		Pages 48

Abstract

The behavior of magnesium potassium phosphate cement (MKPC) pastes or mortars under leaching was investigated in WP4, sub-task 6-3, with two main objectives:

(1) compare the behavior of MKPC pastes / mortars prepared with different fillers (fly ash, and/or blast furnace slag) under leaching by demineralized water or by an alkaline solution representative of the pore solution of conventional concrete placed in the near field of the cemented waste packages;

(2) understand and model the degradation processes of the MKPC matrix under well-controlled conditions.

This report summarizes the main results obtained at KIPT, Ukraine, and CEA, France.

Two complementary approaches were implemented.

- **"Operational" approach**: Following ANS 16.1 standard, some leaching tests were carried out on MKPC mortars prepared with different fillers (fly ash (reference), blast furnace slag, or a mix (50/50) of the two components). The leachability indices and diffusivities of the different species released in solution were calculated from their cumulative concentrations in the leachates. Whatever the filler used, the leachability indices of K, Mg, P and B (LI>9) largely exceeded the LI index threshold of 6 defined by the US Nuclear Regulatory Commission. Blast furnace slag was shown to be an interesting filler, leading to denser materials than fly ash, and thus allowing, in most cases, to slow down the release of elements in the leachates.
- **"Comprehension" approach**: Leaching was performed on MKPC paste samples (reference formulation – fly ash used as a filler) under semi-dynamic and well-controlled conditions (pH maintained constant at 7 or 13.2, renewal of the leaching solution, nitrogen atmosphere, and temperature regulated at 25°C). The compositions of the leachates and solids (from the leached surface to the sound core) were characterized as a function of the leaching time using a large panel of techniques.

  At pH 7, leaching was mainly governed by diffusion of dissolved species through the pore network of the paste. An interface retreat of the solid was observed. K-struvite was fully dissolved close to the exposed surface of the samples. Then, in an intermediate zone, K-struvite coexisted with cattiite.

  At pH 13.2, a layer of Ca-deficient hydroxyapatite (CDHA) rapidly formed on the exposed surfaces and its thickness increased with the leaching duration. However, it was not sufficient to clog the porosity and protect the samples from further degradation. K-struvite dissolved near the exposed surface. In the intermediate zone, it mainly coexisted with brucite, CDHA and a hydrotalcite-like phase.

  Based on these results, a first modeling approach based on reactive transport was proposed. Despite the simplified composition of the paste used for calculations, the model succeeded to reproduce the main mineralogical changes observed experimentally.

Coordinator contact

Maria Oksa
VTT Technical Research Centre of Finland Ltd
Kivimiehentie 3, Espoo / P.O. Box 1000, 02044 VTT, Finland
E-mail: maria.oksa.@vtt.fi
Tel: +358 50 5365 844

Acknowledgement

This project has received funding from the Euratom research and training programme 2019-2020 under grant agreement No 945098.

TABLE OF CONTENTS

1 Introduction

Some legacy radioactive wastes containing aluminum (Al) metal still need to be stabilized and solidified before their final disposal. Currently, Portland cement (PC) is extensively used for the conditioning low- or intermediate-level radioactive waste [1]. However, the high alkalinity of PC leads to strong corrosion of Al metal, which is associated with significant dihydrogen release [2,3]. Therefore, it is important to investigate alternative binders that show better chemical compatibility with Al metal. Magnesium potassium phosphate cements (MKPCs), comprising equimolar amounts of MgO and KH_2PO_4, are interesting candidates since their pore solution pH may fall within the passivation domain of Al metal. The understanding of their long-term durability, especially under alkaline conditions, is however incomplete. Most data are relative to materials with Mg/P molar ratio higher than 1 (the ratio of the reference formulation investigated in WP4-6) and / or prepared using $(NH_4)H_2PO_4$ instead of KH_2PO_4. The objectives of the leaching studies carried out in WP4 Task 6-3 are twofold:

(1) assess the behaviour of MKPC pastes / mortars prepared with different fillers (fly ash, and/or blast furnace slag) under leaching by demineralized water (reference) or by an alkaline solution mimicking the pore solution of conventional concrete placed in the near field of the cemented waste packages;

(2) understand and model the degradation processes of the MKPC matrix under well-controlled conditions. These results should help assessing the extent of degradation of the material as a function of time and pH.

Two experimental approaches were used, involving two contributors.

- "Operational" approach, using ANSI ANS 16.1 test. The leachability indices and diffusivities were calculated from the cumulative concentrations of the different species released in solution. The results obtained for different MKPC formulations were compared between each other, depending on the filler used (fly ash, blast furnace slag, or a mix of the two).
  Contributor: KIPT, Ukraine

- "Comprehension" approach. Leaching was performed under semi-dynamic and well-controlled conditions (pH maintained constant, renewal of the leaching solution, controlled atmosphere and temperature). Both the composition of the leachates and of the solids (from the leached surface to the sound core) were characterized as a function of time. These results were then used as input data for reactive transport modelling.

  Contributor: CEA, France

This report summarizes the results obtained using these two approaches.

2 State of the art

Magnesium potassium phosphate cements (MKPCs) are formed through the reaction between MgO and KH_2PO_4, a soluble acidic phosphate salt [4, 5, 6, 7]. In equimolar amounts, the hydration of MKPCs leads to the formation of K-struvite ($MgKPO_4 \cdot 6H_2O$), a mineral with low solubility that can exist in both crystalline and poorly crystalline (amorphous) forms. The formation of K-struvite sets the pore solution pH to nearly neutral values, falling within the passivation domain of Al metal [3, 7, 8]. Furthermore, various phases like newberyite ($MgHPO_4 \cdot 3H_2O$), phosphorrösslerite ($MgHPO_4 \cdot 7H_2O$), bobierrite ($Mg_3(PO_4)_2 \cdot 8H_2O$), and cattiite ($Mg_3(PO_4)_2 \cdot 22H_2O$) have been identified during the hydration process [7, 9, 10].

While MKPCs hold promise for stabilizing waste with Al metal, there is still limited information on their long-term durability. Lahalle *et al.* [11] investigated the evolution of MKPC paste samples (Mg/P molar ratio of 1 and w/c of 0.56) immersed **in deionized water** (pH 6.8) for 6 months. XRD analyses revealed a decrease in crystalline K-struvite content and an increase in amorphous, likely due to the formation of poorly crystalline K-struvite. Pore solution analyses indicated the release of ions into the immersion solution, particularly K^+ ions. Several studies evidenced a reduction in the compressive strength of magnesium phosphate cement-based materials exposed to water [12, 13, 14, 15]. For instance, Yang *et al.* [12] studied the water resistance of MPC mortars (prepared with $NH_4H_2PO_4$ and a Mg/P molar ratio of 3). These mortars, initially cured for 28 days under endogenous conditions, exhibited a strength decrease of about 11 % and 18 % after 30 and 90 days of immersion, respectively.

Lahalle *et al.* [11] also investigated the evolution of MKPC paste samples (Mg/P atomic ratio of 1) immersed **in alkaline solutions** (containing K, Na and Ca) with and without chlorides (pH 13.2 and 13.3, respectively). XRD analyses showed a decrease in the crystalline content of K-struvite, the precipitation of brucite and an increase in the amorphous content. These authors also suggested the substitution of K^+ by Na^+ in the structure of K-struvite, leading to the formation of hazenite ($Mg_2KNa(PO_4)_2 \cdot 14H_2O$). Furthermore, pore solution extractions showed an increase in pH from 8 to 11-12. In a recent study, Xu *et al.* [16] used thermodynamic modeling to predict the evolution of MKPC pastes (Mg/P molar ratio of 4) exposed to alkaline solutions. K-struvite was calculated to dissolve partly to form brucite and hazenite, which was then confirmed experimentally. Some questions remain however concerning the rate of degradation of MKPC-based materials and the mechanisms controlling this degradation under such alkaline conditions.

These results suggest that the microstructure of MKPC-based materials may vary in contact with water. Therefore, it is not only important to determine their confinement properties, but also to understand their degradation mechanisms under leaching, which will open up prospects for improving their durability**.**

3 Leaching of MKPC cement pastes using ANSI ANS 16.1 test

KIPT, Ukraine, was engaged in the implementation of WP 4.6 and participated in an experimental campaign to change the filler of the reference formulation. KIPT was also associated to the study of the influence of mineralogical additives on the structure and physico - mechanical properties of MKPC materials (4.6.2 - Cost optimization), as well as on their leaching behaviour (4.6.3 – MKPC under leaching). The main objective was to study the leaching behaviour of MKPC materials prepared with different fillers (blast furnace slag (BFS), fly ash (FA), or a mix of the two components) following ASTM ANS 16.1 procedure (American Nuclear Society Standard "Measurement of Leachability in Solidified Low-Level Radioactive Waste by the Short-Term Procedure") [17]. Considering that BFS, along with FA, is a widely available and inexpensive material at metallurgical plants in Ukraine, the use of BFS as mineral additives in the production of MKPC compounds is very promising. The mortar compositions investigated in this study are summarized in Table 1.

Table 1: *Use of BFS in reference formulation.*

Reference formulation			KIPT formulation	
Component	Wt. %		Component	Wt. %
MgO	6,47		MgO	6,47
KH_2PO_4	21,85		KH_2PO_4	21,85
Sand	28,33		Sand	28,33
Fly ash (FA)	28,33	→	3 options: FA, BFS and (½ FA+½ BFS)	28,33
Boric acid	0,57		Boric acid	0,57
Water	14,45		Water	14,45

3.1 Initial materials

The chemical composition of FA from the Burshtyn thermal power plant (Burshtyn, Ukraine) and BFS from the Mariupol metallurgical plant (Mariupol, Ukraine) is shown in Table 2.

Table 2: *Chemical composition of the fly ash and blast furnace slag.*

Industrial waste	Weight content, wt. %										
	SiO_2	Al_2O_3	Fe_2O_3	CaO	MgO	SO_3	C	MnO	TiO_2	$(K,Na)_2O$	Other
FA	46.12	18.00	22.17	4.09	1.46	0.21	2.50	0.14	1.78	2.10	1.43
BFS	38.20	4.60	1.65	48.5	4.3	–	–	0.81	–	0.82	1.12

The raw materials used to prepare the MKPC specimens had the following characteristics: calcined magnesium oxide (MgO > 97 %, particle size < 200 µm); potassium dihydrogen phosphate (KH_2PO_4 > 98 %, size < 630 µm); Sand (SiO_2 > 99.3 %, size < 400 µm); FA (size < 400 µm); BFS (size < 630 µm).

3.2 Preparing specimens

The production of solid MKPC specimens is based on the formation reaction of magnesium potassium phosphate hexahydrate $MgKPO_4$ $6H_2O$ (K-struvite):

$$MgO + KH_2PO_4 + 5\ H_2O \rightarrow MgKPO_4 \cdot 6H_2O + Q_{heat} \quad \text{(Eq. 1)}$$

In accordance with the KIPT proposed formulation, the MKPC specimens were prepared with different fillers (for a total content of 28.33 wt. % of the reference formulation): MKPC with FA filler (further referred as MKPC – FA), MKPC with BFS filler (MKPC – BFS) and MKPC with ½ FA+½ BFS filler (MKPC – FA – BFS). To manufacture these specimens, the dry mixtures were first prepared by mixing MgO, KH_2PO_4, sand and filler in a lab grinding mill machine (Fritch, single pulverising porcelain bowl of 200 g capacity, Ø2.0 cm aluminum oxide balls, speed 150 rpm, mixing time 10 minutes). Then, boric acid H_3BO_3, used as a reaction retarder, was dissolved in distilled water, and the mixture of dry components was added to this solution and mixed with a mechanical stirrer in a 250 ml polypropylene can for 5 minutes until a homogeneous paste was obtained. Finally, the mortar was poured into polypropylene moulds and covered with polyethylene film to prevent rapid drying. Cubic specimens with dimensions of 3×3×3 cm were demoulded after 1 day and kept for at least 28 days to cure in indoor ambient conditions.

3.3 Characterization

3.3.1 XRD

The crystalline phase composition of all obtained MKPC based specimens cured for 28 days was studied by X-ray diffraction analysis (XRD) (DRON-4-07 device using copper Cu-K_α radiation and a Ni selective absorbing filter). Crystalline phase quantification was performed using MAUD (Materials Analysis Using Diffraction) software to analyse diffraction data using the combined Rietveld method.

Analysis of the XRD data for MKPC - FA, MKPC - BFS, and MKPC – FA - BFS specimens shows that the content of K-struvite in the crystalline fraction of the three mortars is almost the same and is equal to 58-60 % (Table 3).

Table 3. *Quantitative phase composition of MKPC specimen prepared with different fillers.*

Composition	Phase	%	Lattice parameters, Å
MKPC – FA (28.33 wt.%)	Quartz	38	a=4,912; c=5,398
	$MgKPO_4 \cdot 6H_2O$	58	a=6,875; b=6,160; c=11,083
	Mullite	4	a=7,583; b=7,650; c=2,886
MKPC – BFS (28.33 wt.%)	Quartz	31	a=4,913; c=5,414
	$MgKPO_4 \cdot 6H_2O$	60	a=6,897; b=6,188; c=11,109
	Akermanite	9	a=7,783; c=5,028
MKPC – FA – BFS (½FA+½BFS) = 28.33 wt.%	Quartz	34	a=4,913; c=5,402
	$MgKPO_4 \cdot 6H_2O$	59	a=6,874; b=6,158; c=11,091
	Akermanite	7	a=7,773; c=5,020

MKPC - BFS sample is characterized by the presence of K-struvite with higher crystal lattice parameters, as comparison to both MKPC - FA and MKPC – FA - BFS samples. This indicates that, during the preparation of MKPC - BFS mortar, a more significant dissolution of the BFS particles

occurs, releasing various elements that are included in the K-struvite crystal structure with an increase in its crystal lattice parameters. The observation of the mullite phase ($Al_6Si_2O_{13}$) in MKPC-FA specimen is explained by its presence in initial FA powder (Figure 1-a). Similarly, akermanite ($Ca_2MgSi_2O_7$) observed in both MKPC – BFS and MKPC – FA – BFS specimens is a component of the BFS powder (Figure 1-b).

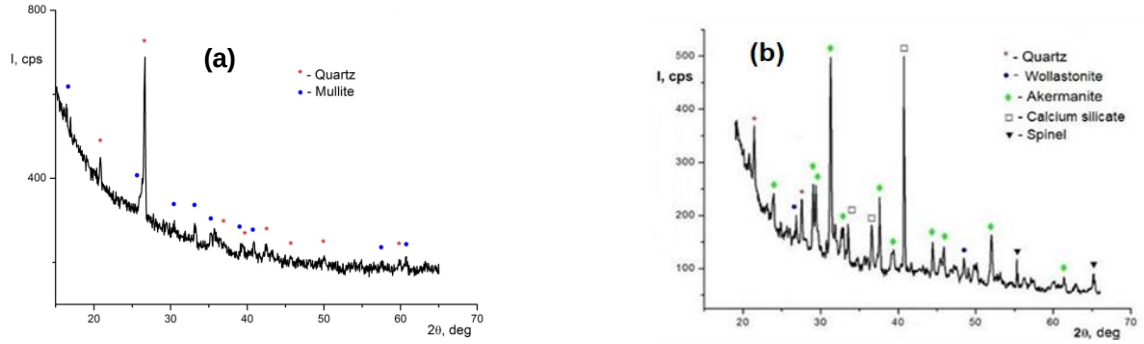

Figure 1. *Diffraction patterns of initial filler materials: a – initial FA powder, b – initial BFS powder.*

3.3.2 Microstructure

The microstructure of specimens was observed using scanning electron microscopy (JSM-6510 microscope) and SEM images of the microstructure of MKPC-based mortars after 28 days of curing are presented in Figure 2.

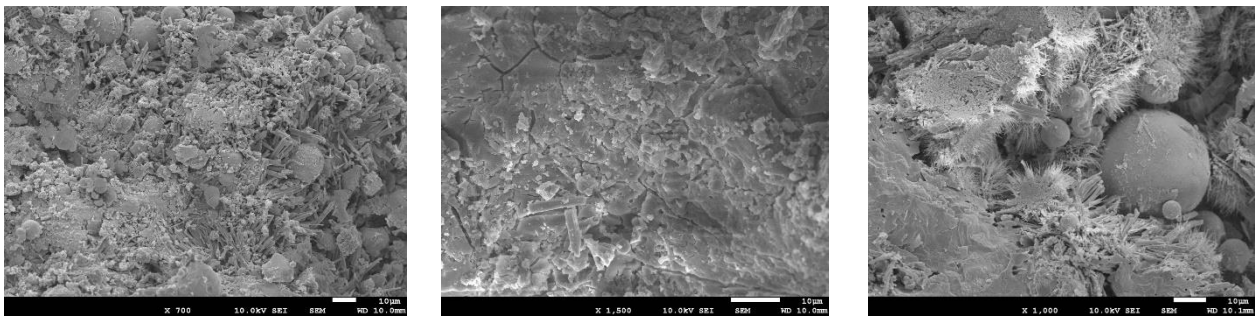

a b c

Figure 2. *SEM images of obtained specimens: a – MKPC with FA filler, b - MKPC with BFS filler, c - MKPC with filler (½ FA+½ BFS).*

The matrix material of all specimens contains K-struvite crystals in the form of prisms and needles. In addition, encapsulated spherical FA particles are present in MKPC-FA and MKPC-FA-BFS. The presence of unreacted FA spherical particles is explained by the fact that FA particles are heterogenous in terms of composition and size, as already reported by other authors [18, 19]. This results in different reactivities for individual FA powder particles.

In general, MKPC – BFS specimens have a denser structure compared to MKPC – FA specimens. The structure is more uniform. Crystals of K-struvite in the form of well-cut prisms are observed. The presence of microcracks is caused by dehydration of the specimen under vacuum during SEM observation. The microstructure of MKPC-FA-BFS sample is more complex than that of MKPC – FA, but seems less dense than that of MKPC – BFS.

3.4 Leaching procedure

Leaching tests were performed according to ANS 16.1 by immersing the specimen for 90 days in distilled water contained in a 1-liter HDPE (High Density Polyethylene) vessel, ensuring that all sides of the specimen are in contact with the leachant (Figure 3).

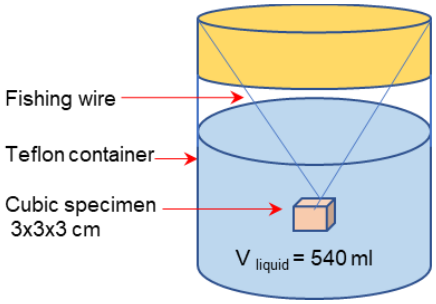

Figure 3: *Placing the specimen in a HDPE vessel.*

Leaching tests were carried out at a temperature of 25 °C. The leachate was sampled, and the fresh leachant was replaced after increasing leaching periods, i.e., 1, 4, 14, 28 and 43 days. The test thus lasted 90 days (1+4+14+28+43 days). From the results of the leaching tests, the leaching characteristics of the different elements from the solidified MKPC specimens were evaluated based on their cumulative concentrations in the leachates. The effective diffusion coefficient (D_e) and leachability index (LI) were also calculated to quantitatively evaluate whether the MKPC matrix can be used for waste conditioning.

The concentrations (mg/L) of the major elements (K, Mg, P) and B leached from the MKPC specimens were analysed using an inductively coupled plasma atomic emission spectroscope (ICP–AES, iCAP 6300 Duo, Thermo Scientific Corporation). Also, the mineralogical and structural characteristics of the samples before and after leaching were studied.

The measured element concentrations were used to plot cumulative concentrations (CC) versus time and calculate leachability indices. Leachability index (LI) for each element was determined based on the following expressions according to ANS-16.1:

$$LI = \frac{1}{5}\sum_{1}^{5} [\log(\beta/D_e)]_n \quad \text{(Eq. 2)}$$

where β is a defined constant (1.0 cm^2/s).

D_e can be calculated using the mass transport equation (i.e., Fick's second law) as follows:

$$D_e = \pi \left[\frac{a_n/A_o}{(\Delta t)_n}\right]^2 \left[\frac{V}{S}\right]^2 T \quad \text{(Eq. 3)}$$

where D_e is the effective diffusion coefficient (cm^2/s), V is the volume of the specimen (cm^3), S is the geometric surface area of the solid specimen (cm^2), a_n is the amount of element released from the specimen for the n-th leaching interval, A_o is the initial amount of the element in the specimen prior to leaching, $\Delta t_n = t_n - t_{n-1}$ is the duration of the n-th leaching interval, and T is the leaching time representing the mean time (s) of the n-th leaching interval for a semi-infinite medium:

$$T = \left[\frac{1}{2}\left(\sqrt{t_n} + \sqrt{t_{n-1}}\right)\right]^2 \quad \text{(Eq. 4)}$$

3.5 Results of leaching tests

3.5.1 Leaching in distilled water

Specimens based on MKPC mortars were prepared and subjected to leaching tests in distilled water. However, it was not possible to measure the concentrations in the leachates, since the KIPT Institute was partially destroyed and closed due to the outbreak of war by Russia. Only after a six-month pause, it was possible to continue research on leaching at KIPT. And the main thing that was discovered is that the previously prepared specimens retained their shape and integrity after 1 year of aging in distilled water. Their appearance is presented in Figure 4.

Figure 4. *Specimens after 1 year of aging in distilled water, from left to right: MKPC - FA, MKPC – BFS and MKPC – FA - BFS.*

Further, at KIPT it was still possible to continue research work on leaching tests for a new batch of MKPC-based specimens. The results are given below.

As shown in Figure 5, the cumulative concentrations (CC) of elements constantly increased with time. Potassium (K) had the highest CC value compared to other elements for all specimens.

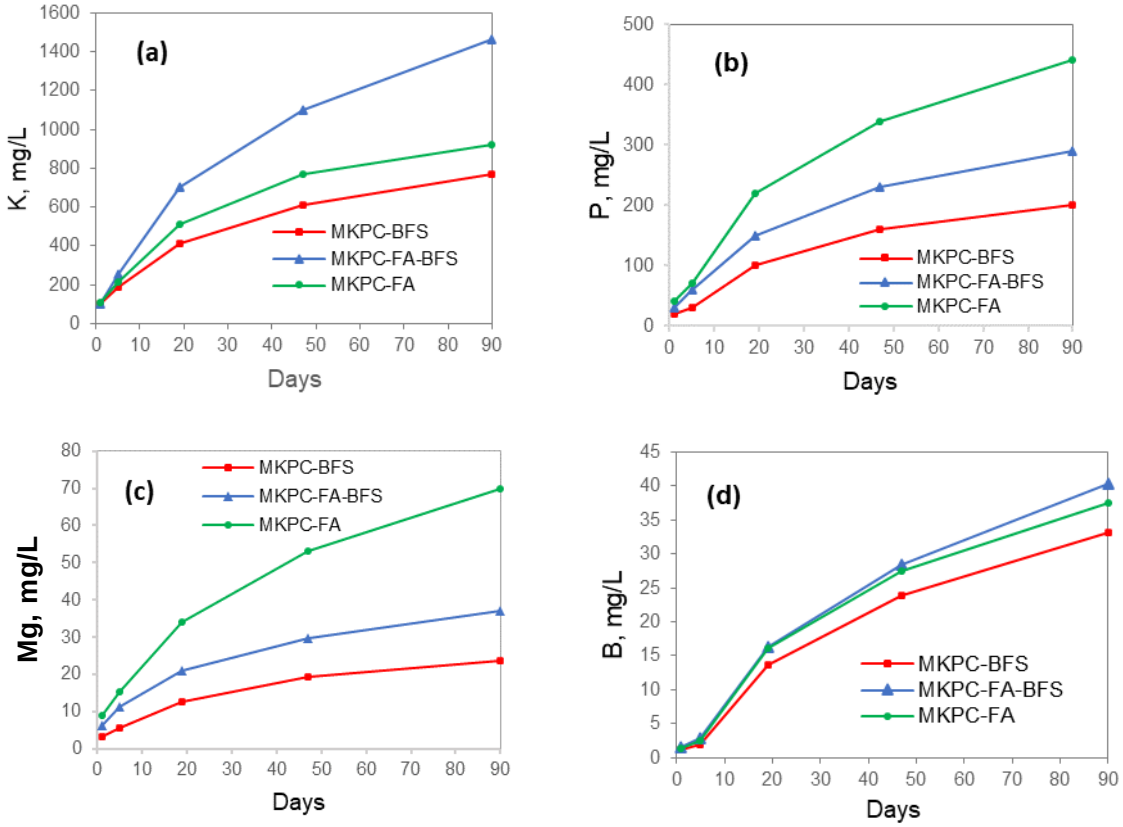

Figure 5. *Cumulative concentrations of leached elements: a – K, b – P, c – Mg and d – B.*

The concentrations of MKPC matrix elements in the leachates for all specimens check the relationship: K > P > Mg > B (Figure 5). It should be noted that residual KH_2PO_4, which did not react following reaction (1), as well as fly ash (Table 2) which is used as a filler in the production of MKPC – FA and MKPC – FA – BFS specimens, contribute to the high release of K into the leachates (Figure 5-a).

The reduced leaching of P and Mg from MKPC matrix with BFS additives (MKPC – FA - BFS and MKPC – BFS), compared to the MKPC - FA specimen (Figure 5-b, c), might be explained by the formation of persistent phases on the surface of the specimens during the leaching process, such as bobierrite $Mg_3(PO_4)_2 \cdot 8H_2O$, and dolomite - calcium magnesium carbonate $CaMg(CO_3)_2$, evidenced on the XRD patterns (Figure 6-a, b, c), but also by the denser microstructure of this sample.

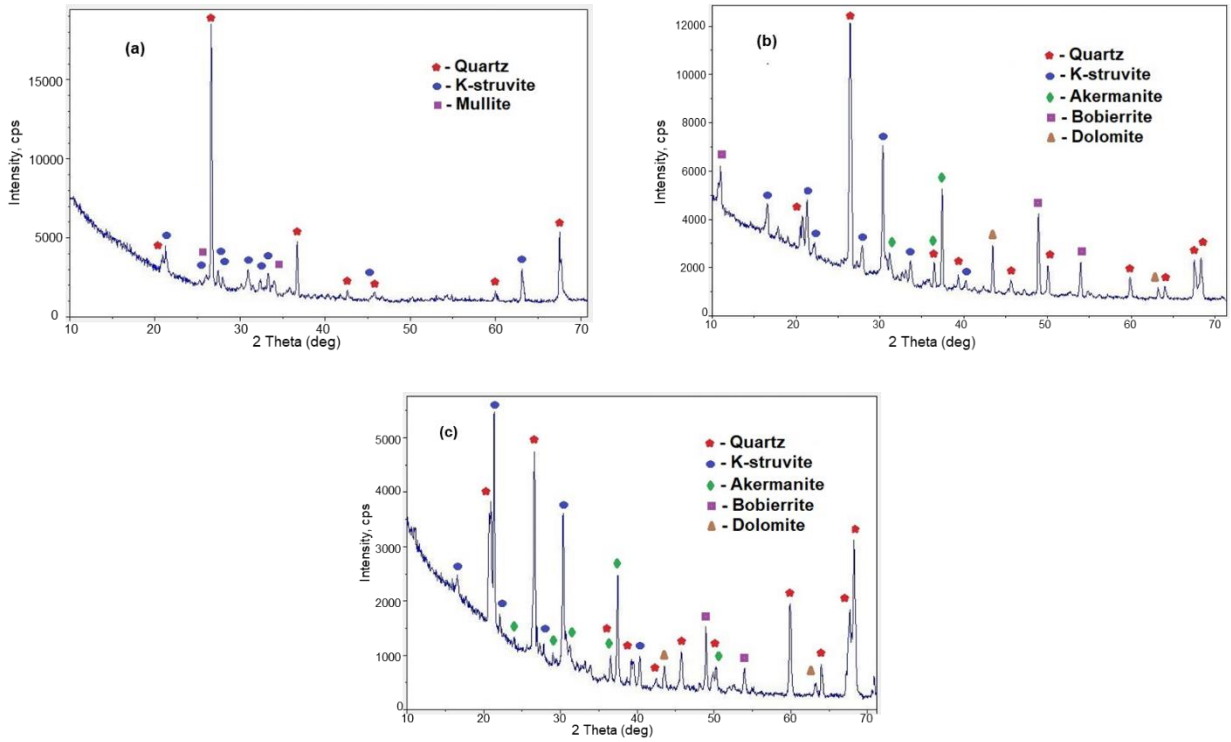

Figure 6. *XRD patterns after leaching test (90 days): a – MKPC - FA, b – MKPC – FA - BFS, c – MKPC – BFS.*

The CC values for B are approximately the same (Figure 5 d) for all specimens and relatively high, given its low initial content in the samples (Table 1).

Regarding the SEM study of leached materials, it should be noted that, whatever their composition, the materials retained their structure. No defects in the form of chips and cracks were detected after 90 days of leaching. It should be noted that after leaching, K-struvite crystals are visible on the surface of the samples, the shape of which has changed compared to the original (Figure 2). The edges have become more rounded. This is caused by their partial dissolution, which is clearly visible on the (MPC – BFS) material (Figure 7). Similar changes in the shape of K-struvite crystals after exposure to aqueous water for 60 days were also observed in [20].

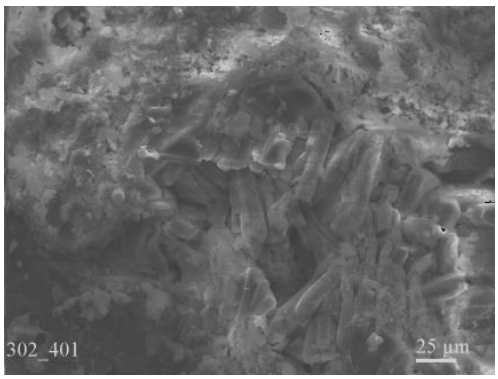

Figure 7. *SEM image of the surface microstructure in MKPC - BFS specimen after 90 days of leaching.*

Based on the measured element concentrations, effective diffusion coefficients D_e and leachability indices LI were calculated (Table 4). These data are necessary to assess the behaviour of waste forms under conditions of constant water saturation, which simulate disposal conditions under the most conservative scenario.

Table 4. *Effective diffusion coefficients D_e and leachability indices LI of elements (leaching by distilled water).*

Element	D_e (cm^2s^{-1}) and LI					
	MKPC-BFS		MKPC-FA-BFS		MKPC-FA	
	D_e	LI	D_e	LI	D_e	LI
K	$5{,}31 \cdot 10^{-10}$	9,61	$1{,}47 \cdot 10^{-9}$	9,15	$6{,}78 \cdot 10^{-10}$	9,50
P	$3{,}86 \cdot 10^{-11}$	10,61	$8{,}91 \cdot 10^{-11}$	10,29	$1{,}65 \cdot 10^{-10}$	9,97
Mg	$8{,}29 \cdot 10^{-13}$	12,39	$3{,}41 \cdot 10^{-12}$	11,91	$8{,}26 \cdot 10^{-12}$	11,36
B	$5{,}21 \cdot 10^{-10}$	9,60	$1{,}76 \cdot 10^{-9}$	8,99	$1{,}42 \cdot 10^{-9}$	9,06

For comparison, in [21], devoted to the use of magnesium potassium phosphate cement for the immobilization of nickel-containing waste, the leachability index for K calculated according to the ANS 16.1 test was 9.9. The highest LI values are obtained for MKPC - BFS specimen. Its better chemical resistance can result from its denser initial microstructure, as compared to that of MKPC - FA and MKPC - FA - BFS samples (Figure 2).

3.5.2 Leaching in synthetic cementitious water

The purpose of the test is to assess the behaviour of MKPC pastes / mortars when leached by an alkaline solution representative of the pore solution of conventional concrete placed in the near field of the cemented waste packages. It uses a defined reference protocol for short-term testing, including minimum requirements for the characterization of liquids and solids.

Leaching tests of MKPC specimens were carried out in “CEM I + silica fume” synthetic water, prepared using the following recipe : for 1 liter solution, add 0.9798 g Na_2SO_4, 0.2666 g $CaCl_2$, 15.2 mL 1M NaOH, 16.6 mL 1M KOH. Such solution had a pH of 12.6.

Leaching tests in alkaline solution were carried out according to the conditions of standard ANS 16.1. Concentration values for leached potassium were determined by subtracting the concentration in the original alkaline solution from the resulting concentrations in the leachates. Note that the solution initially contained potassium at a concentration of 571.2 mg/L measured by ICP-AES.

After leaching in an alkaline solution for 90 days, the specimens retained their integrity and shape (Figure 8), but limited precipitation of white salts was noticed on the surface of the specimens.

Figure 8. *MKPC - FA, MKPC - BFS and MKPC – FA - BFS specimens (from left to right) after leaching in an alkaline solution for 90 days.*

The concentrations of matrix elements released in the leachates for all specimens checked the following relationship: K > P > B > Mg (Figure 9, a-d).

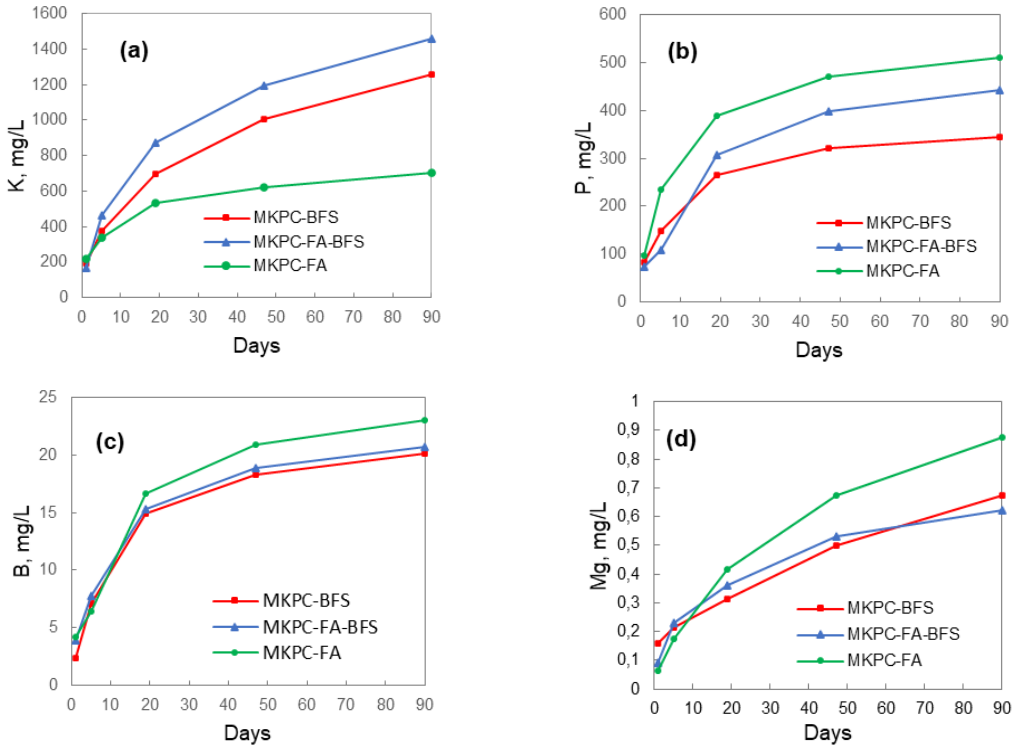

Figure 9. *Cumulative concentrations of leached elements in alkaline solution: a – K, b – P, c – B and d – Mg.*

In contrast to distilled water, the Mg CC in the alkaline solution decreases significantly and becomes smaller than that of B (Figure 9-c, d). The highest release of K from MKPC matrix is observed with MKPC – FA - BFS specimen, whatever the leaching solution (distilled water or alkaline solution (Figure 5-a, Figure 9-a). However, the smallest release of K in the alkaline solution is observed with MKPC - FA specimen, instead of MKPC – BFS specimen in distilled water. Releases of P from MKPC matrices leached by demineralized water or by the alkaline solution are almost of the same magnitude order (Figure 5-b, Figure 9-b). Table 5 shows the calculated effective diffusion coefficients and leachability indices.

Table 5. *Effective diffusion coefficients D_e and leachability indices LI for elements released in alkaline solution.*

Element	D_e (cm^2s^{-1}) and LI					
	MPC-BFS		MPC-FA-BFS		MPC-FA	
	D_e	LI	D_e	LI	D_e	LI
K	$1{,}59 \cdot 10^{-9}$	9,17	$3{,}29 \cdot 10^{-9}$	9,06	$9{,}49 \cdot 10^{-10}$	9,74
P	$1{,}19 \cdot 10^{-10}$	10,15	$1{,}90 \cdot 10^{-10}$	10,00	$3{,}51 \cdot 10^{-9}$	9,8
B	$1{,}34 \cdot 10^{-9}$	9,29	$2{,}28 \cdot 10^{-9}$	9,27	$2{,}70 \cdot 10^{-9}$	9,24
Mg	$7{,}98 \cdot 10^{-16}$	15,49	$1{,}56 \cdot 10^{-15}$	15,45	$1{,}27 \cdot 10^{-15}$	15,19

The US Nuclear Regulatory Commission has defined a minimum value of six (6.0) for the leachability index as an acceptance criteria for radioactive waste forms to be disposed of at controlled sites [22], i.e., the leachability index, as calculated in accordance with ANS 16.1, should be greater than 6. The leaching tests carried out in this work according to the ANSI/ANS 16.1 standard show that this requirement is checked for the main elements (K, Mg, P) of the MKPC matrices, regardless of the leaching solution (distilled water or alkaline solution). Indeed, the leaching indices are ≥9 (Table 4, Table 5). This means that it seems possible to use blast furnace slag, in addition or substitution to fly ash, as a filler in MKPC materials, which is extremely important for Ukrainian needs [23].

4 Understanding the leaching behavior of MKPC paste in neutral and alkaline solutions

The work presented hereafter is the result of a post-doctoral study carried out at CEA/LFCM (Marcoule, France) and CEA/LECBA (Saclay, France) in the framework of WP4, sub-task 6-3. This work aimed at understanding (by experimental and numerical approaches) the leaching behavior of magnesium potassium phosphate cement (MKPC) paste samples under well-controlled conditions. Two different leaching solutions were used: demineralized water (pH maintained at 7) and an alkaline solution (pH 13.2). MKPC paste samples were prepared using equimolar amounts of MgO and KH_2PO_4. After six months of endogenous curing, semi-dynamic leaching tests were performed on monoliths. Leaching solutions were periodically renewed and leachates were analyzed by ICP-AES. Degradation mechanisms were assessed by microstructural and mineralogical analyses performed on solid samples before and after leaching, using different experimental techniques (XRD, SEM/EDS, RAMAN, MAS-NMR). Furthermore, experimental data were used as input for numerical simulations using HYTEC reactive transport code.

4.1 Materials and methods

4.1.1 Raw materials

The raw materials used in this study are presented in Table 6.

Table 6. *Raw materials used in WP4 task 6.3 – "comprehension" approach.*

Raw material	**MgO**	**KH_2PO_4**	**Low calcium oxide fly ash**	**$B(OH)_3$**
Description	Hard-burnt magnesium oxide purchased from Martin Marietta Magnesia specialties (MagChem® 10CR). Purity = 98.3 %. Particle size distribution: d_{10} = 4.8 µm, d_{50} = 18.9 µm, d_{90} = 45.6 µm, Specific surface area (BET) = 0.9 m^2/g.	Potassium dihydrogen phosphate purchased as a fertilizer from YARA, Krista™. Purity > 98 %. Particle size distribution: d_{10} = 139 µm, d_{50} = 303 µm, d_{90} = 566 µm	Siliceous fly ash (class V according to EN 197-1) obtained from EDF (power station from Cordemais, France) and used to improve the rheological properties and stability of the mixtures. Particle size distribution: d_{10} = 7 µm, d_{50} = 31 µm, d_{90} = 163 µm Specific surface area (BET) = 1.5 m^2/g. Phase composition determined by XRD and Rietveld refinement: 72.4 wt.% amorphous, 17.2 wt.% mullite and 10.4 wt.% quartz.	Boric acid purchased from VWR (reference number 20177). Purity > 98 % Used as a set retarder.

The chemical compositions of MgO, KH_2PO_4 and fly ash were determined using semi-quantitative X-ray fluorescence (XRF) with a Bruker S.8 spectrometer and are presented in Table 7.

Table 7. *Chemical compositions of the raw materials, obtained by semi-quantitative XRF. Values are given in % by weight.*

	SiO_2	Al_2O_3	Fe_2O_3	CaO	K_2O	TiO_2	Na_2O	MgO	P_2O_5	SO_3	Cl^-
MgO	0.3	-	0.3	0.9	-	-	-	98.5	-	-	-
KH_2PO_4	-	-	-	-	40.0	-	-	-	59.3	0.5	0.1
Fly ash	57.8	24.7	6.0	4.5	2.2	1.3	0.7	1.6	0.6	0.5	0.1

4.1.2 Sample preparation and curing

MKPC paste samples were prepared using the reference formulation established in WP4, as detailed in Table 8. The mix design of MKPC paste samples is presented in Table 9. Moreover, the sequence of paste preparation is schematized in Figure 10.

Table 8. *Formulation used for MKPC paste samples in WP4 task 6.3 – "comprehension" approach.*

Parameter	Mg/P[a]	w/c[b]	Fly ash/c[c]	Boric acid/c[d]
Ratio	1	0.51	1	0.02

[a] *Mg/P molar ratio*
[b] *Water-to-cement (w/c) weight ratio, (cement: MgO + KH_2PO_4)*
[c] *Fly ash-to-cement weight ratio*
[d] *Boric acid-to-cement weight ratio*

Table 9. *Mix design of 1 L MKPC paste.*

	MgO (g)	KH_2PO_4 (g)	Fly ash (g)	Boric acid (g)	Water[a] (g)
MKPC	131.4	443.6	575.0	11.5	293.2

[a] *Demineralized water;* [b] *Water-to-cement weight ratio (cement: MgO+KH_2PO_4).*

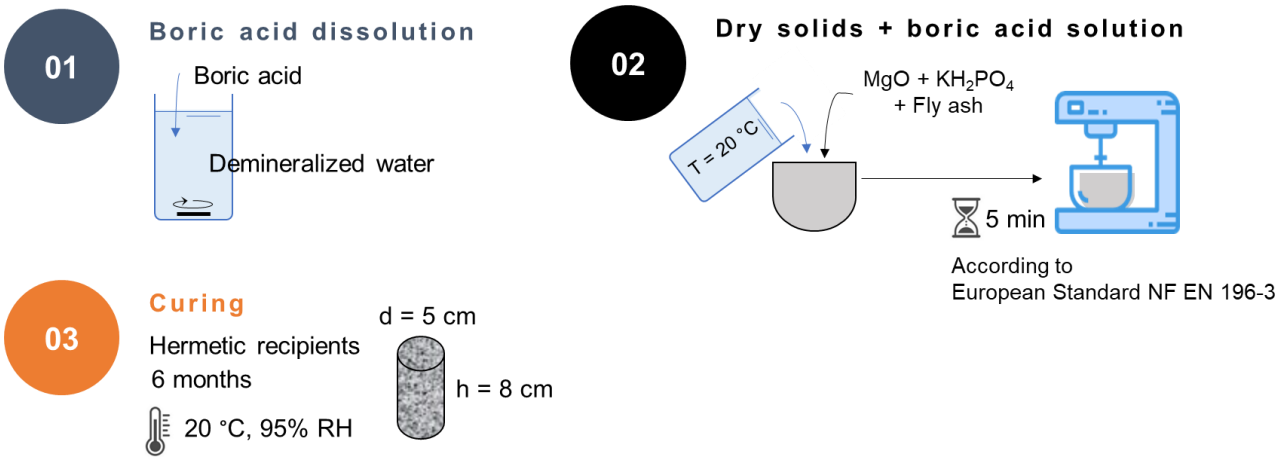

Figure 10. *Sequence of preparation of MKPC paste samples.*

4.1.3 Protocols and characterization techniques

Table 10 summarizes all the characterization techniques used in this study. The different techniques are categorized by goals.

Table 10. *Techniques used to characterize leached samples and leachates composition.*

Goal	Description
Investigation of the porosity and pore size distribution of hardened MKPC paste samples before leaching	**Hydration stoppage:** For the mineralogical and microstructure characterizations, hydration stoppage was performed on pastes after 6 months of curing by solvent exchange using isopropanol and following the RILEM TC-238 SCM guidelines [24]. Residual isopropanol was removed by placing the samples in a desiccator at 20 °C and 20 % R.H. for 7 days. After leaching, MKPC samples were simply rinsed with isopropanol.
	Mercury Intrusion Porosimetry (MIP): MIP analyses were carried out on small pieces of pastes of about 1 g to 3 g previously immersed into isopropanol and dried into a desiccator at 20 °C and 20 % R.H. Analyses were conducted with an AutoPore IV 9500 Porosimeter from Micromeritics Instrument Corporation, following the ISO 15901-1 (2005) standard.
	Total porosity accessible to water: Experiments were performed according to European Standard NF P 18-459 (2022). Different temperatures were used to dry the samples in order to evaluate the stability of K-struvite: 20°C, 25°C, 38°C and 50°C. Porosity was determined using drying conditions at 38°C and 16%R.H. to ensure K-struvite integrity.
Investigation of the mineralogical assemblage and microstructure of MKPC paste samples before and after leaching	**X-ray diffraction (XRD):** XRD analyses were carried out on pastes manually ground to a particle size below 63 µm. All XRD analyses were performed with a PANalytical X'Pert Pro diffractometer using transmission mode. Rietveld analyses were performed to quantify the different crystalline phases and the amorphous fraction using the Fullprof_suite program [25]. During the refinement, multiple profile and structure parameters were allowed to vary, such as zero shift, unit cell parameters, B overall factor, preferred orientation and scale factor. The broadening effect was refined using an anisotropic size model. After refining the content of each phase (wt %), the amount of the amorphous phase was estimated from the ratio between the amount of silicon (used as internal standard) found after the refinement and its real content of 10 wt%. After leaching, XRD analyses were performed on powders recovered at different depths of the leached MKPC samples by scratching their surfaces (from the exposed surfaces to the core). Their final thickness was measured using a digital caliper (range 0-25 mm, digital step 0.001 mm).
	Thermogravimetric analysis (TGA): TGA analyses were conducted using a NETZSCH STA 409 PC equipped with an oven capable of reaching temperatures of up to 1500 °C. The analyses were performed from 30 °C to 1000°C, and the temperature gradually increased at a rate of 10 °C/min.
	Solid state magic angle spinning nuclear magnetic resonance (MAS NMR): MAS-NMR was used to investigate changes in the P, B, Si, Al environments before leaching. After leaching only P and B were investigated. ^{31}P and ^{29}Si spectra were acquired on a Bruker AVANCE III spectrometer (B_0 = 9.4 T) operating at 162 MHz and 79.4 MHz for ^{31}P and ^{29}Si, respectively. For ^{31}P spectra, the spinning speed was fixed at 20 kHz and 384 scans were accumulated after a single short pulse (π/4) and a recycling delay of 360 s ensuring complete magnetization relaxation. In the case of ^{29}Si spectra, the rotation was limited at 8 kHz, and almost 34000 scans were added with a recycling delay of 10 s. ^{27}Al and ^{11}B spectra were obtained on a Bruker AVANCE NEO spectrometer (B_0 = 20 T) operating at 221.6 MHz and 272.8 MHz for ^{27}Al and ^{11}B respectively, using a spinning speed of 30 kHz. ^{27}Al spectrum was acquired after a short pulse (π/18) ensuring a homogeneous excitation, 10240 scans were added using a recycling delay of 1 s. Finally, ^{11}B spectra were acquired using a Hahn-echo pulse sequence to remove the probe signal. 20324 scans were accumulated with a recycling delay of 10 s. Nevertheless, despite the 2.3 days of acquisition time, the spectrum remained very noisy, making accurate quantification impossible. The chemical shifts were referenced relative to H_3PO_4 85%, $BF_3O(C_2H_5)_2$, $Al(NO_3)_3$ and trimethylsilane for ^{31}P, ^{11}B, ^{27}Al and ^{29}Si, respectively. Quantitative analyses of the ^{31}P MAS NMR spectra were performed using the Dmfit program developed at CEMHTI [26].

Goal	Description
	SEM/EDS analyses: The microstructure of MKPC pastes was characterized using Scanning Electron Microscope (SEM) FEI Inspect 50 equipped with an electron dispersive spectroscopy (EDS) detector (Bruker XFlash SDD 10 mm^2). All observations were carried out on carbon-coated fractures and polished sections. EDS point analyses were performed to identify the dissolution or precipitation of phases in the solid fraction, with an average of 150 analyses taken per sample. Calibration for quantification was achieved using a set of eleven reference standards: jadeite $NaAl(Si_2O_6)$, magnesium oxide (MgO, 99.95 % pure), aluminum oxide (Al_2O_3, 99.8 % pure), orthoclase ($KAlSi_3O_8$), wollastonite ($CaSiO_3$), titanium (Ti, 99.99 % pure), chromium (Cr, 99.96 % pure), manganese (Mn, 99.99 %), iron (Fe, 99.95 % pure), pyrite (FeS_2) and gallium phosphide (GaP, 99.99 % pure). Images were obtained in backscattered electron (BSE) configuration, applying magnifications between 50x and 2,000x. After leaching, samples were delicately rinsed with isopropanol and cut into small pieces by using a diamond wire saw. EDS mapping was performed to estimate the degraded layer depth and changes in the elemental composition. Moreover, EDS point analyses were performed from the exposed surface to the core to identify either the dissolution or the precipitation of phases in the solid fraction.
	Raman spectroscopy: Raman spectroscopy was used to investigate vibrational modes of phosphate precipitates. Analyses were performed on powder samples using a Raman XploRA Plus (Horiba) equipped with a Syncerity detector (cooled down at -60°C). Raman spectra were recorded in the 1800-50 cm^{-1} range using 10 accumulations per scan with an acquisition time of 20 s per accumulation. The pairing of laser wavelength and diffraction grating used was 532 nm-1800 gr/mm, with a laser intensity set at 100%.
Study of the leaching behavior or MKPC paste samples	**Preparation of paste samples**: After 6 months of curing, MKPC pastes were cut to obtain cylindrical samples of 2 cm length and 5 cm diameter. To generate unidirectional diffusion through the samples, lateral surfaces of cylindrical samples were covered with an epoxy resin, whereas the parallel extremities were kept unprotected.
	Preparation of semi-dynamic leaching tests: All semi-dynamic leaching tests were carried out in double-walled reactors maintained at 25 °C and previously filled with 1.7 L of leaching solution. The liquid volume-to-solid surface (L/S) ratio was equal to 43.29 cm and magnetic stirring was applied during the whole test to avoid concentration heterogeneities. To avoid carbonation of the solutions, the injection of water-saturated nitrogen (N_2) into the reactors was performed by bubbling. A scheme of the device used is presented in Figure 11.
	Semi-dynamic leaching tests at pH 7: Three different semi-dynamic leaching experiments were carried out on MKPC paste samples using demineralized water and a test duration of 28 days, 90 days and 210 days. The pH of the leaching solutions was controlled at 7 by adding small aliquots of 0.5 M nitric acid (HNO_3) using a titrator (Titroline 7000 using TitriSoft software - version 3.5.0/3.5.0 P) operating in the pH-stat mode.
	Semi-dynamic leaching tests at pH 13: Two different semi-dynamic leaching experiments were carried out on MKPC paste samples using an alkaline solution (pH 13). The tests were carried out for 14 days and 170 days. The alkaline solution aimed at mimicking the pore solution of a conventional concrete (composite cement containing blast furnace slag and fly ash) that might be encountered in the vicinity of the cemented waste package. First, demineralized water was boiled for 1 h at 105 °C to eliminate carbon dioxide (CO_2), and then cooled under nitrogen atmosphere. The decarbonated water was used to prepare a solution containing 0.05 mol/L NaOH, 0.15 mol/L KOH (86%), and 0.001 mol/L CaO (obtained by calcining calcium hydroxide ($Ca(OH)_2$) in a furnace at 1000 °C for 8 h to remove any carbonate traces). Once the reactants were dissolved, the solution achieved a pH of 13.2±0.1. The pH of the leaching solution was not controlled over time. Frequent solution renewals allowed maintaining the pH around 13 all along the tests.

Goal	Description
Determination of leached species in leachates	**ICP-AES analyses:** After each renewal, leachates were filtered at 0.2 µm and elemental concentrations (K, P, Mg, B, Ca, Si, S, Na, Al, Fe, Ti and Mn) were measured by Inductively Coupled Plasma Atomic Emission Spectrometry (ICP-AES). Leachates were diluted by factors of 10 or 100 using diluted HNO_3 (2 vol. % HNO_3 in ultrapure water, 18.2 MΩ.cm).
Estimation of pH in the MKPC paste samples before and after leaching	A pH-indicator was used to estimate the pH of cement pastes before and after leaching. To this end, the Rainbow indicator was purchased from German Instruments. This indicator has broad pH range: orange (pH 4-6), yellow (pH 6-8), green (pH 8-10), purple (pH 10-12), and blue (pH 12-14). In order to measure the pH of paste samples, the indicator was sprayed on the cross-section of either broken pieces or cut samples. Pictures of sprayed surfaces were taken after a few minutes when the indicator solution was dried.

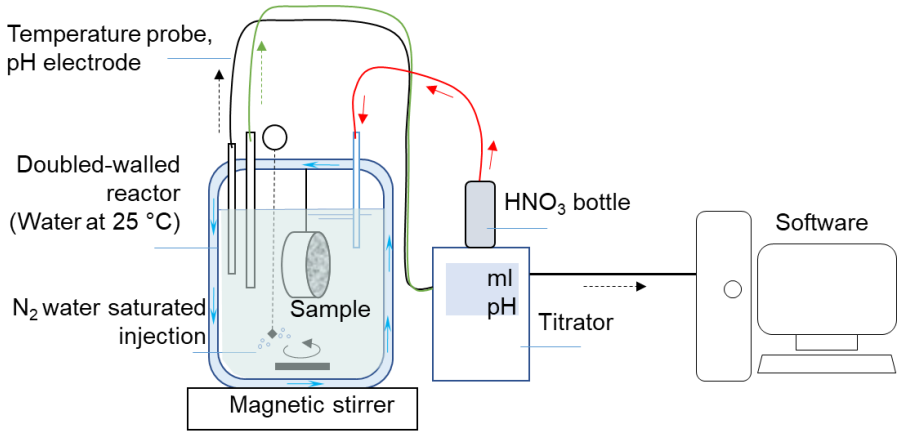

Figure 11. *Scheme of the device used for leaching tests. Titrator was only used for leaching tests at pH 7.*

4.1.4 Modeling

The leaching behavior of MKPC paste samples was simulated using a one-dimension (1D) coordinate model developed with reactive transport code HYTEC, version 4.7.4 [27]. In this code, diffusion is coupled to chemistry following equation (Eq. 5) [28]:

$$\frac{\partial \omega c_i}{\partial t} = \nabla.(D_e \nabla c_i) - \frac{\partial \omega \bar{c}_i}{\partial t} \qquad \text{(Eq. 5)}$$

c_i: mobile concentration of a species per unit volume of solution,
$\bar{c}_i$: immobile concentration,
ω: porosity, and
D_e: effective diffusion coefficient.

Therefore, the model considers simultaneously the chemical evolution of the pore solution, the mineralogical alteration fronts induced by sequential dissolution/precipitation of the cement hydration products, and the release of elements from the cement paste. Furthermore, alterations in local porosity due to mineral precipitation or dissolution lead to changes in the D_e value. To incorporate the retroactive effect of chemistry on mass transport, a modified version of Archie's law was implemented in the HYTEC code, as described by equation (Eq. 6) [28]:

$$D_e(\omega) = D_e(\omega_0)\left(\frac{\omega-\omega_c}{\omega_0-\omega_c}\right)^{\alpha} \quad \text{(Eq. 6)}$$

ω: porosity,
D_e: effective diffusion coefficient,
ω_0: initial porosity (determined experimentally),
ω_c: critical porosity threshold under which diffusion stops, set to 0 in the calculations,
α: empirical Archie's coefficient.

According to the literature, Archie's coefficients ranging from 1.5 to 4 have been commonly used to model the degradation of cementitious materials [28, 29, 30, 31]. In this study, an Archie's power of 2.0 provided satisfactory fit of the experimental results. Figure 12 illustrates the computational domain defined in this study, which comprised two zones: *(i)* the MKPC paste sample, and *(ii)* the reactor containing the leaching solution. The node sizes of the calculation grid were set at 100 µm in the paste and in the first 10 mm of the reactor zone, and at 1 mm elsewhere in the reactor. No boundary conditions were defined in this model. Additionally, the leaching solution was renewed at the same frequency as in the experiments.

For modeling of leaching tests carried out with demineralized water, the pH of the solution (water) was set at 7. For modeling of the tests performed under alkaline conditions, the composition of the leaching solution was defined as follows: 0.13 mol/L KOH, 0.05 mol/L NaOH and 0.001 mol/L $Ca(OH)_2$. In both cases, a diffusivity coefficient of 1.0×10^{-5} $m^2 \cdot s^{-1}$ was used to simulate a homogeneous and agitated solution.

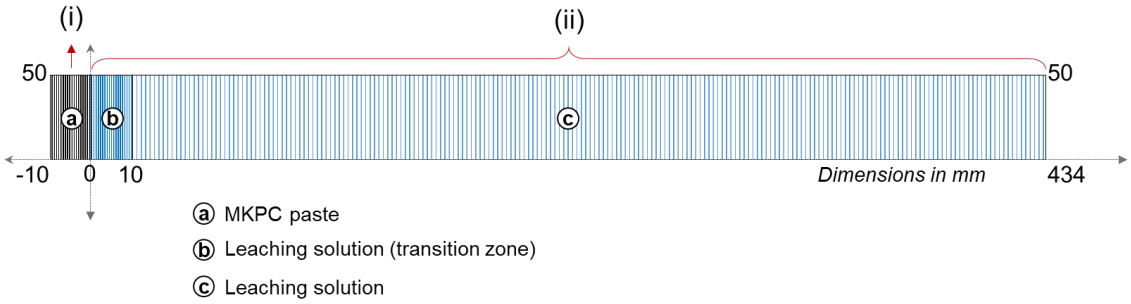

Figure 12. *Scheme of the 1D computational domain including (i) MKPC paste, and (ii) the reactor zone containing the leaching solution. Node size grid:* ***(a), (b)*** *100 µm, and* ***(c)*** *1 mm.*

The chemical reactions were computed by assuming local thermodynamic equilibrium and utilizing the B-dot activity model for ionic strength correction. The thermodynamic CHESS database (version 2.5) was used in these simulations and enriched with thermodynamic data for magnesium phosphate phases. The minerals considered in the model are summarized in Table 11.

Table 11. *Thermodynamic data at 25 °C and 1 bar.*

Species	Reaction	Log $K_{formation}$	Vol (kg/m^3)	Ref.
K-struvite	$Mg^{2+} + HPO_4^{2-} + K^+ + 6H_2O \rightarrow MgKPO_4{\cdot}6H_2O + H^+$	-1.36	1870.2	[10]
Cattiite	$3Mg^{2+} + 2HPO_4^{2-} + 22H_2O \rightarrow Mg_3(PO_4)_2.22H_2O + 2H^+$	-1.61	1640.5	[10]
$Mg_2KH(PO_4)_2.15H_2O$	$2Mg^{2+} + 2HPO_4^{2-} + K^+ + 15H_2O \rightarrow Mg_2KH(PO_4)_2.15H_2O + H^+$	4.03	1810.6	[10]
Phosphorrösslerite	$Mg^{2+} + HPO_4^{2-} + 7H_2O \rightarrow MgHPO_4.7H_2O$	4.69	1740.3	[10]
Newberyite	$Mg^{2+} + HPO_4^{2-} + 3H_2O \rightarrow MgHPO_4.3H_2O$	5.61	2121.1	[10]
$MgKPO_4.H_2O$	$Mg^{2+} + HPO4^{2-} + K^+ + H_2O \rightarrow MgKPO_4.H_2O + H^+$	-1.37	2668.7	[10]
Farringtonite	$3Mg^{2+} + 2HPO_4^{2-} \rightarrow Mg_3(PO_4)_2 + 2H^+$	-2.23	2761.2	[10]
Bobierrite	$3Mg^{2+} + 2HPO_4^{2-} + 8H_2O \rightarrow Mg_3(PO_4)_2{\cdot}8H_2O + 2H^+$	0.66	2129.9	[10]
Magnesium orthophosphate tetrahydrate	$3Mg^{2+} + 2HPO_4^{2-} + 4H_2O \rightarrow Mg_3(PO_4)_2{\cdot}4H_2O + 2H^+$	-1.14	2380.6	[10]
Lünebergite	$3Mg^{2+} + 2HPO_4^{2-} + 2B(OH)_3 + 6H_2O \rightarrow Mg_3B_2(PO_4)_2(OH)_6{\cdot}6H_2O + 2H^+$	-99.25	-	[32]

4.2 Experimental results

4.2.1 Characterization of MKPC paste samples after curing and before leaching

4.2.1.1 XRD and TGA analyses

XRD analyses indicated that the MKPC paste samples contained crystalline K-struvite ($MgKPO_4{\cdot}6H_2O$), residual MgO, quartz, mullite, and an amorphous content (Figure 13-a). Quartz and mullite were present in the fly ash added to the mixture. The amorphous content was attributed to the glassy content of the fly ash, but also to the potential presence of transient magnesium phosphate phases and/or poorly crystallized K-struvite [8, 11]. The mineralogical assemblage comprised 53.8 wt% K-struvite, 1.8 wt% MgO, 8.2 wt% mullite, 2.6 wt% quartz, and 33.6 wt% amorphous, as estimated by XRD Rietveld refinement.

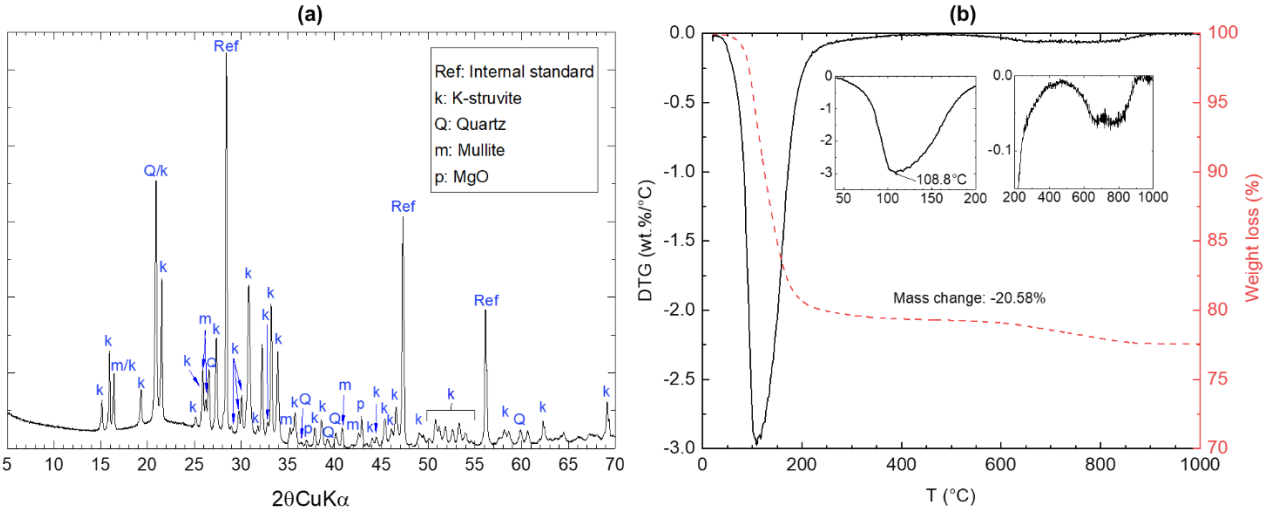

Figure 13. *MKPC paste after 6-months of curing* ***(a)*** *XRD pattern, and* ***(b)*** *TGA analyses, right axis: weight loss given in percentage, and left axis: first derivative of weight loss given in wt.%/K.*

TGA analyses exhibited a weight loss from 100 °C to 400 °C, attributed to the dehydration of magnesium phosphate phases such as K-struvite and $Mg_2KH(PO_4)_2{\cdot}15H_2O$, as previously reported in the literature [9, 33] (Figure 13-b). This weight loss was centered at around 109 °C, suggesting the primary presence of K-struvite. Moreover, a weight loss between 600 °C and 800 °C was observed and potentially linked to traces (< 1%) of carbonates (such as magnesium carbonates like nesquehonite $MgCO_3{\cdot}3H_2O$ [34]), formed due to sample carbonation during preparation.

4.2.1.2 SEM/EDS analyses

Figure 14-a presents a SEM image obtained from the polished MKPC paste sample. The presence of K-struvite was abundant and characterized by micro-cracks likely resulting from drying due to the high vacuum in the SEM chamber. Some fly ash grains were also observed all over the MKPC matrix. Some darker grey zones indicated the presence of residual MgO.

Figure 14-b shows a mixing diagram built from EDS data, in which Mg/P and K/P atomic ratios were plotted in the x- and y-axis, respectively. This figure also presents the expected regions for the different phases that could be present during hydration of the MKPC matrix (*e.g.,* K-struvite, $Mg_2KH(PO_4)_2{\cdot}15H_2O$, brucite, bobierrite, cattiite, phosphorrösslerite, newberyite) [10, 33].

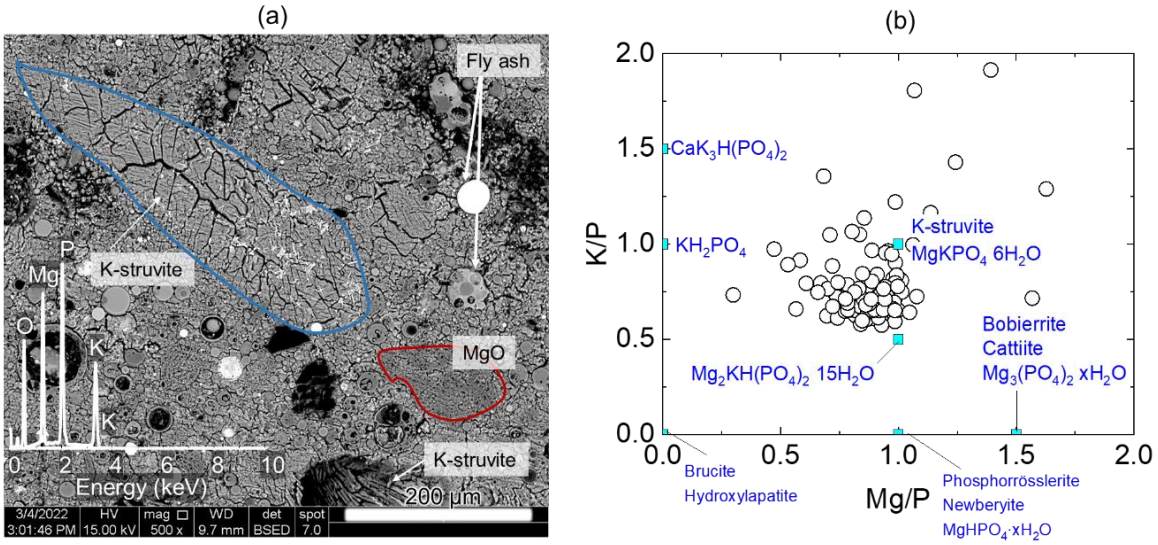

Figure 14. (a) *SEM image by BSE from a polished section of MKPC paste, and* ***(b)*** *EDS mixing diagram of K/P vs Mg/P atomic ratios.*

EDS points deviated from the Mg/P and K/P ratios of 1 expected for K-struvite. This suggested the coexistence, at the submicronic level, of K-struvite and $Mg_2KH(PO_4)_2{\cdot}15H_2O$ (in which the Mg/P and K/P atomic ratios are 1 and 0.5, respectively), or other poorly crystalline phosphate phases with reduced Mg or K content which could not be evidenced by XRD.

4.2.1.3 MAS NMR spectroscopy

Figure 15 and Figure 16 show the ^{31}P, ^{29}Si and ^{27}Al MAS-NMR spectra obtained from the MKPC paste after 6 months of endogenous curing.

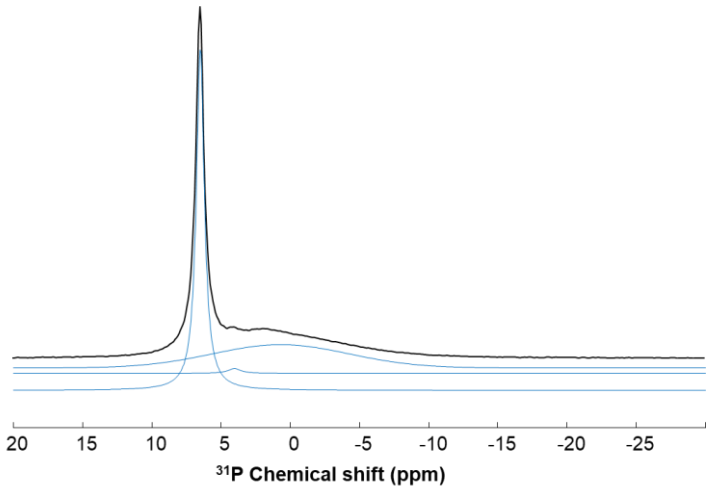

***Figure 15**. [31]P MAS-NMR of MKPC paste before leaching.*

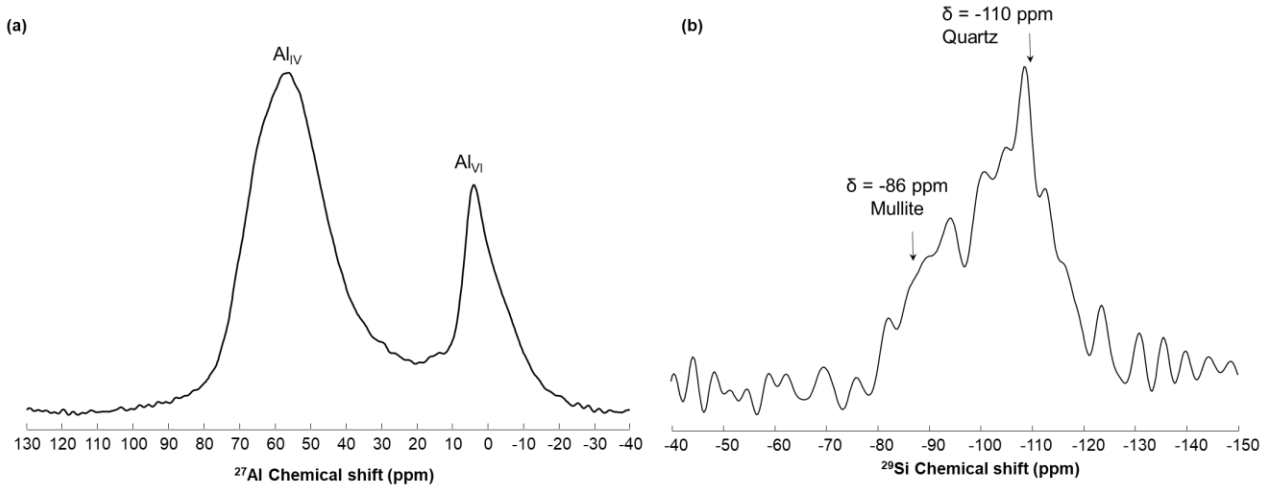

***Figure 16**. MKPC paste before leaching **(a)** [29]Si MAS NMR, and **(b)** [27]Al MAS NMR spectra. δ indicates chemical shift.*

The ^{31}P spectrum displayed three distinct signal contributions corresponding to different P chemical environments (Figure 15). The dominant sharp signal at δ = +6.5 ppm was assigned to K-struvite (76% of the ^{31}P fraction), in agreement with literature reports [18, 33, 35]. The small resonance at δ = +4.1 ppm was associated with residual KH_2PO_4 [18, 33] (1% of the ^{31}P fraction), indicating that after 6 months of curing, KH_2PO_4 was not completely exhausted. The broad hump signal, centered at δ = +0.9 ppm, was not clearly assigned to any specific compound. However, it may correspond to one or several contributions of poorly crystallized phosphate phases, such as:

(i) $Mg_2KH(PO_4)_2{\cdot}15H_2O$, δ = +2.6 ppm, +3.1 ppm, +3.4 ppm, and +3.7 ppm [33],

(ii) lünebergite ($Mg_3B_2(PO_4)_2(OH)_6{\cdot}6H_2O$), δ = - 2.7 ppm [33],

(iii) a poorly crystallized anhydrous or hydrated orthophosphate ($Mg_3(PO_4)_2$, δ = +0.6 ppm to δ = -0.5 ppm [35]; $Mg_3(PO_4)_2{\cdot}xH_2O$), δ = -0.73 ppm, -0.89 ppm, - 2.69 ppm, and -3.03 ppm [36]).

The ^{27}Al NMR spectrum showed the presence of Al in 4-fold coordination (δ = +51 ppm) and 6-fold coordination (δ = +1 ppm) (Figure 16-a). It is well-known that both Al environments are present in fly

ash, the octahedral site corresponding more precisely to mullite [37]. On the ^{29}Si NMR spectrum (Figure 16-b), the signal extended from -80 to -115 ppm. Due to the low signal/noise ratio, only the thin signal of quartz (δ = - 110 ppm) was clearly distinguished. The rest of the signal corresponded to the different silicon environments of the vitreous part of fly ash and to mullite [37, 38].

4.2.1.4 Porosity of MKPC paste samples

Figure 17 and Figure 18 present the total porosity accessible to water and mercury, as well as the pore size distribution in MKPC paste samples before leaching.

The total porosity accessible to mercury (15.2 %) was consistent with the total porosity accessible to water (15.5 ±0.2 %). The distribution of pore entry diameters revealed that MKPC paste presented a wide range of pore size diameters (Figure 18). The highest population of pore size diameters (31%) ranged between 0.01 and 0.1 µm, meanwhile 11% of the distribution corresponded to large pore size diameters (> 100 µm).

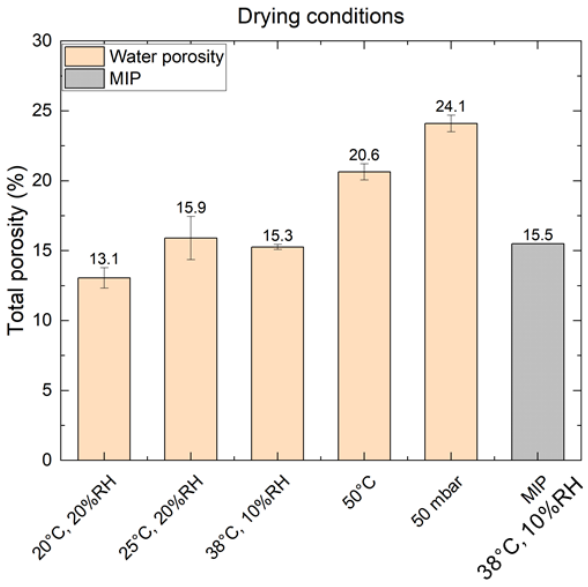

***Figure 17**. Total porosity determined in MKPC paste samples as a function of the drying temperature.*

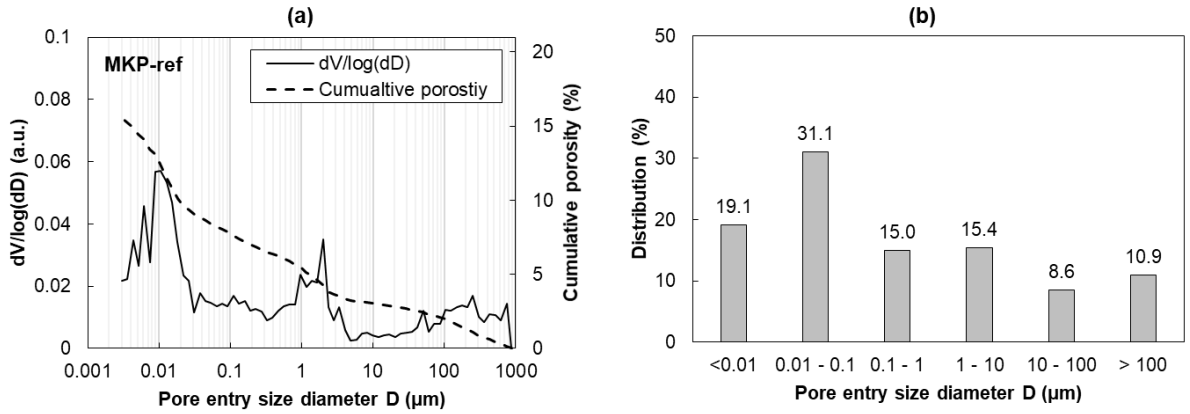

***Figure 18. (a)** Cumulative MIP porosity and first derivative results, and **(b)** distribution of the pore entry size diameter in MKPC paste before leaching.*

4.2.2 Leaching of MKPC paste samples by demineralized water (pH 7)

4.2.2.1 Evolution of leached species in solution

Figure 19 presents the evolution of the cumulative leached concentrations (in mmol/L) of K, P, Mg, B, S, Si and Ca as a function of the square root of time (in days$^{1/2}$) for leaching tests carried out for 28, 90 and 210 days. Table 12 displays the initial composition of the MKPC paste sample along with the cumulative leached elemental concentrations (in mmol/g of paste) determined for all leaching periods. The data were calculated using a density value of 1,876.2 kg/m^3 for the cement paste (obtained from total porosity accessible to water experiments).

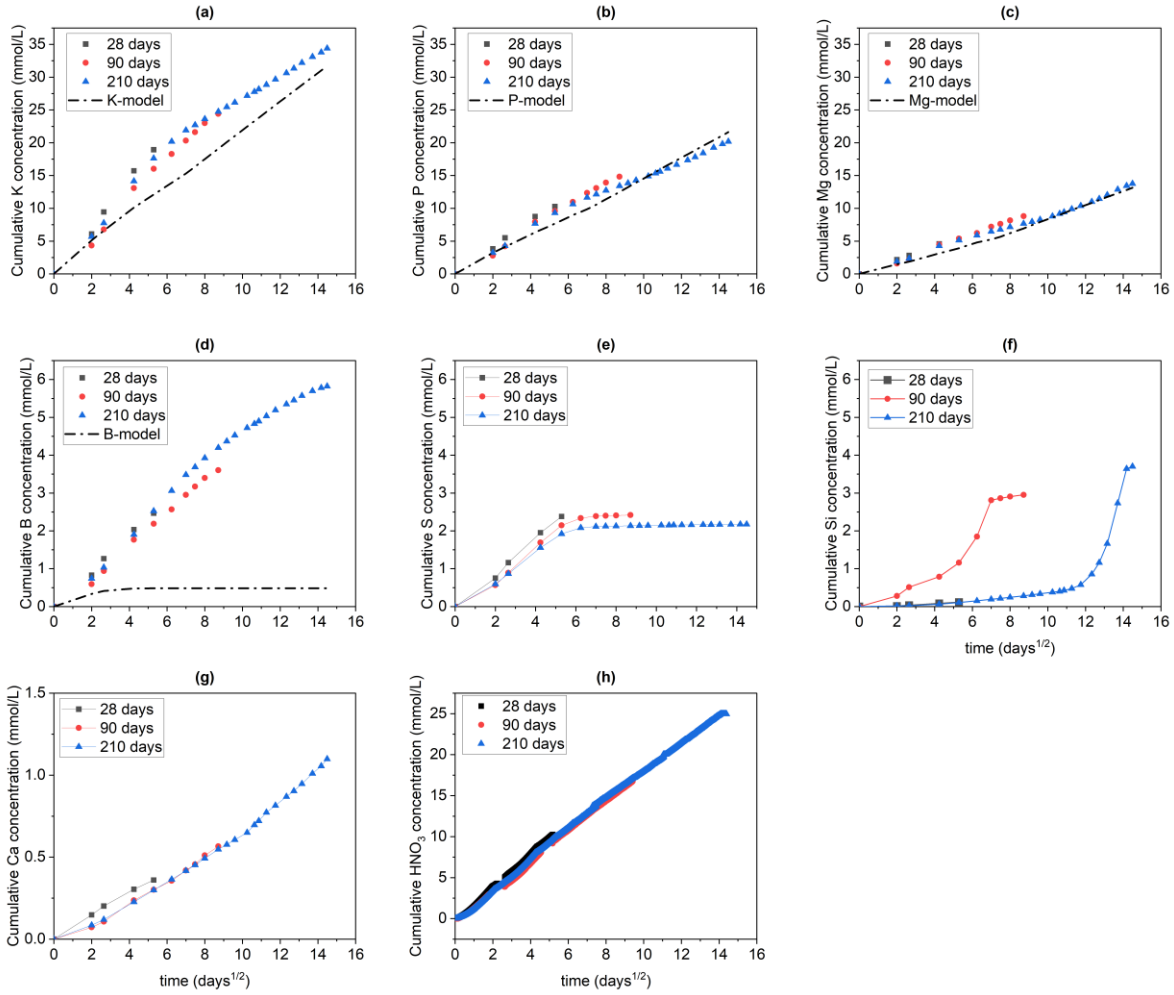

Figure 19. *Cumulative concentrations (in mmol/L) of leached species as a function of the square root of time (in days$^{1/2}$). (a) K, (b) P, (c) Mg, (d) B, (e) S, (f) Si, (g) Ca, and (h) HNO_3 injected by titration. Dots: experimental results, dashed lines: concentrations calculated with the reactive transport model.*

***Table 12**. Initial and leached elemental concentrations (in mmol/g of paste) and leached fractions (in mol%).*

			Al	B	Ca	Fe	K	Mg	Na	P	S*	Si
		Initial concentration	1.9	0.1	0.3	0.6	2.8	2.4	0.1	2.6	0.0	3.8
Leaching time (days)	28	Leached concentration	0.0	0.1	0.01	0.0	0.4	0.1	0.003	0.2	0.1	0.003
		Leached fraction (%)	0.0	43.1	2.5	0.0	15.8	5.1	4.0	9.2	130.8	0.1
	90	Leached concentration	0.0	0.1	0.01	0.0	0.6	0.2	0.01	0.3	0.1	0.1
		Leached fraction (%)	0.0	62.9	3.9	0.0	20.3	8.6	6.6	13.2	132.8	1.8
	210	Leached concentration	0.0	0.13	0.03	0.0	0.79	0.32	0.01	0.47	0.05	0.09
		Leached fraction (%)	0.0	101.7	7.6	0.0	28.6	13.4	8.8	18.0	119.5	2.2

**Note that the experimental error associated to S concentration determination by ICP-AES was significant (c.a. 15%), resulting in a cumulative leached fraction higher than 100% for this element.*

Figure 19 showed the good repeatability of the leaching experiments carried out on MKPC paste samples, except for the quantification of Si in the leachates, possibly due to heterogeneities in the soluble fraction of fly ash. Leaching by demineralized water at pH 7 resulted in a continuous release of elements into the solution, leading to a gradual increase of elemental concentrations in the leachates The leaching of K was considerably higher than that of P, which in turn exceeded that of Mg. B and S were completely depleted from the matrix at the end of the longest leaching experiment, meaning that the minerals containing S and B were highly soluble.

As shown in Figure 19-h, the cumulative concentration of HNO_3 injected by titration increased linearly with the square root of time, indicating the release of basic aqueous species such as PO_4^{3-} and OH^-. Similar linear evolutions were observed for the cumulative concentrations of Mg, Ca, as well as S and B until their exhaustion from the solid. As for K and P, two linear regimes were successively observed, with a change occurring after 28 days of leaching. This transition could result from the exhaustion of dissolved species in the pore solution and soluble phases containing K and/or P, such as residual KH_2PO_4, accounting for 1 mol.% of the ^{31}P fraction (Figure 15). In addition, leaching of soluble K present in fly ash or in impurities could also be involved during the first 28 days.

Regardless of the test duration, the K/Mg and P/Mg flux ratios (equal to ≈3.6 and ≈2.0, respectively - Table 13) strongly deviated from 1, thus indicating that the release of Mg, K and P did not simply result from congruent dissolution of K-struvite $MgKPO_4.6H_2O$, but resulted from a combination of different reactions.

***Table 13.** Regression analyses of cumulative concentrations of K, P, Mg and B in the leachates during the first 28 days of leaching, using the method of least squares. Slopes (S) are reported in mmol·L^{-1}·$d^{-1/2}$ along with their corresponding standard deviations (S.D.) and correlations coefficients (r^2).*

Test	1			2			3		
Element	Slope	S.D.	r^2	Slope	S.D.	r^2	Slope	S.D.	r^2
K	3.695	0.154	0.993	2.920	0.099	0.995	3.394	0.153	0.992
P	1.998	0.026	0.999	1.742	0.043	0.998	1.796	0.063	0.995
Mg	1.020	0.026	0.997	0.982	0.044	0.992	0.991	0.038	0.994
B	0.478	0.015	0.996	0.397	0.012	0.996	0.480	0.031	0.983
K/P	1.8			1.7			1.9		
K/Mg	3.6			3.0			3.4		
P/Mg	2.0			1.8			1.8		

1, 2 and 3 refer to the leaching tests carried for 28, 90 and 210 days. Note that, for comparison, the slopes were calculated by using only the first five points of each curve presented in Figure 19.

4.2.2.2 Mineralogical evolution of leached solids

Hereafter, MKPC paste samples recovered after 28, 90 and 210 days of leaching will be referred to as MKP-28d, MKP-90d and MKP-210d, respectively.

After leaching, MKPC paste samples were recovered and their thickness was measured using a digital caliper. All the exposed surfaces were friable, and the epoxy resin was easily removed, without any observed cracking or swelling (Figure 20). The thickness of leached samples decreased over time, meaning that surface erosion occurred, leading to progressive loss of material and interface retreat (interface = exposed surface). The interface retreat (0.55 mm ± 0.15 mm, 1.32 mm ± 0.16 mm, and 2.08 mm ± 0.17 mm for MKP-28d, MKP-90d and MKP-210d, respectively) seemed to increase linearly with the square root of time. Extrapolating this trend would lead to an interface retreat of approximately 2.6 mm after 1 year of leaching.

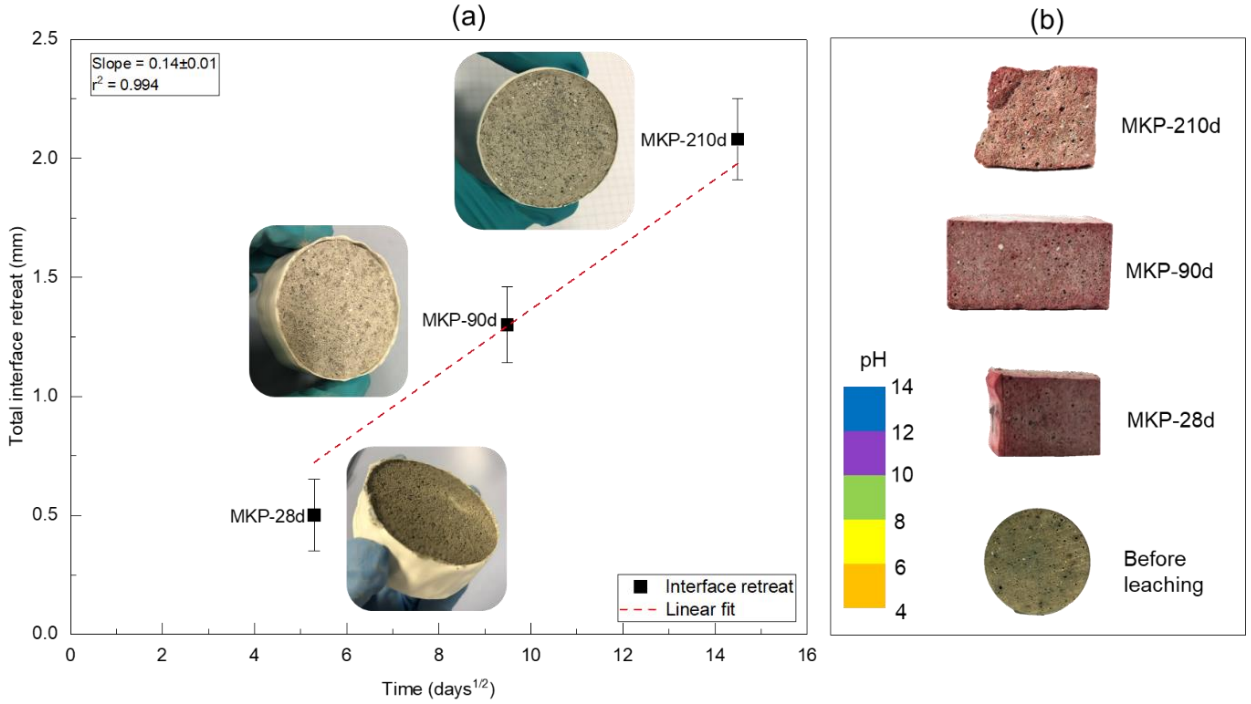

Figure 20. *MKPC paste samples before and after leaching. Left: Interface retreat of leached solids (in mm) versus the square root of time (in days$^{1/2}$). Slope is given in mm·d$^{-1/2}$. The value of interface retreat includes the two exposed surfaces in the leached samples. Right: estimation of pH on the cross-section of leached samples using the Rainbow indicator.*

4.2.2.3 XRD analyses of leached solids

XRD analyses (Figure 21) of leached solids indicated a zonation process in the MKPC pastes. Three main zones were detected.

- Zone 1 was found at the exposed surfaces of the samples and was characterized by a residual layer of variable thickness (0 to around 200-300 µm). XRD patterns indicated the presence of mullite, quartz and an amorphous fraction. K-struvite was not detected in this zone.

- Zone 2 extended from 300 µm to 1.5 mm in MKP-28d, and was observed until a depth of *c.a.* 2.8 mm and 3.0 mm in MKP-90d and MKP-210d, respectively. This intermediate zone was composed of K-struvite, mullite, quartz, amorphous, as well as cattiite, a potassium-free magnesium phosphate phase ($Mg_3(PO_4)_2 \cdot 22H_2O$).

- Zone 3 did not contain cattite anymore, and its composition was close to that of the pristine cement paste.

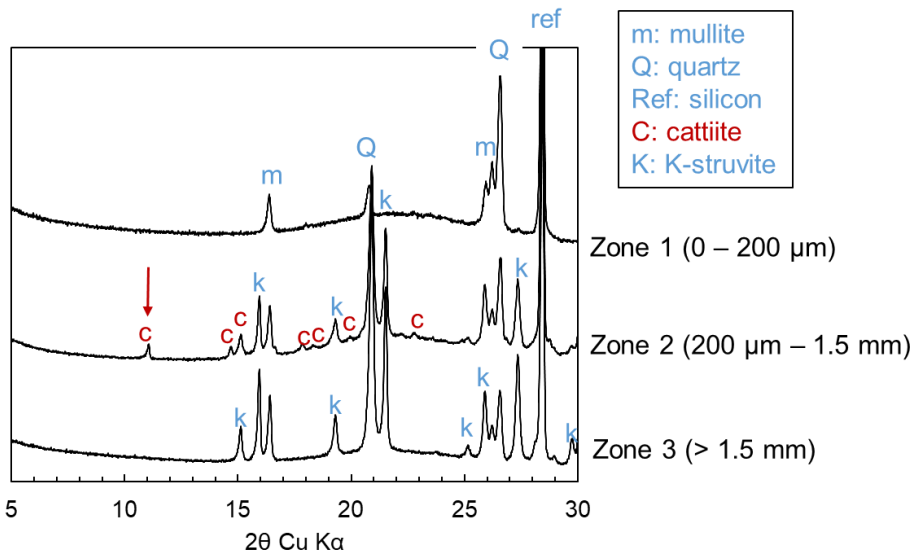

Figure 21. *XRD patterns of MKP-28 d sample leached at pH 7.*

Figure 22 presents a SEM image obtained from the 90-day leached solid and the corresponding EDS elemental maps. The white dotted line helps to distinguish the residual layer observed in the sample. It was mainly composed of fly ash, as confirmed by EDS mapping of Al and Si (Figure 22). The SEM image also showed some darker grey regions in zone 2, with lower concentrations in K, but still containing Mg and P. This result was consistent with the precipitation of cattiite.

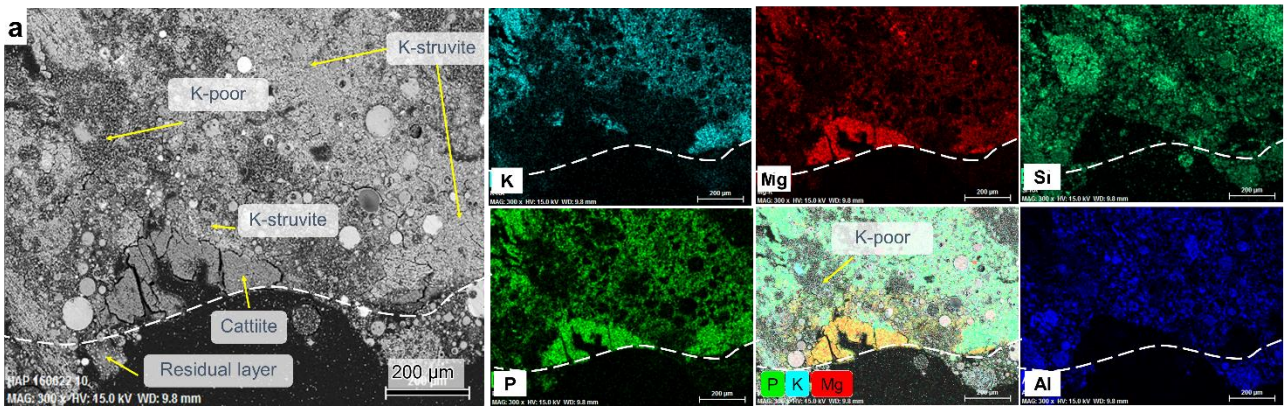

Figure 22. *SEM/EDS analyses of MKP-90d sample leached at pH 7 (zones 1 and 2).*

EDS point analyses obtained after leaching in the residual layers and intermediate zones of MKP-28d, MKP-90d and MKP-210d are presented in Figure 23 and compared to the results obtained with the pristine paste sample (see section 4.2.1.2).

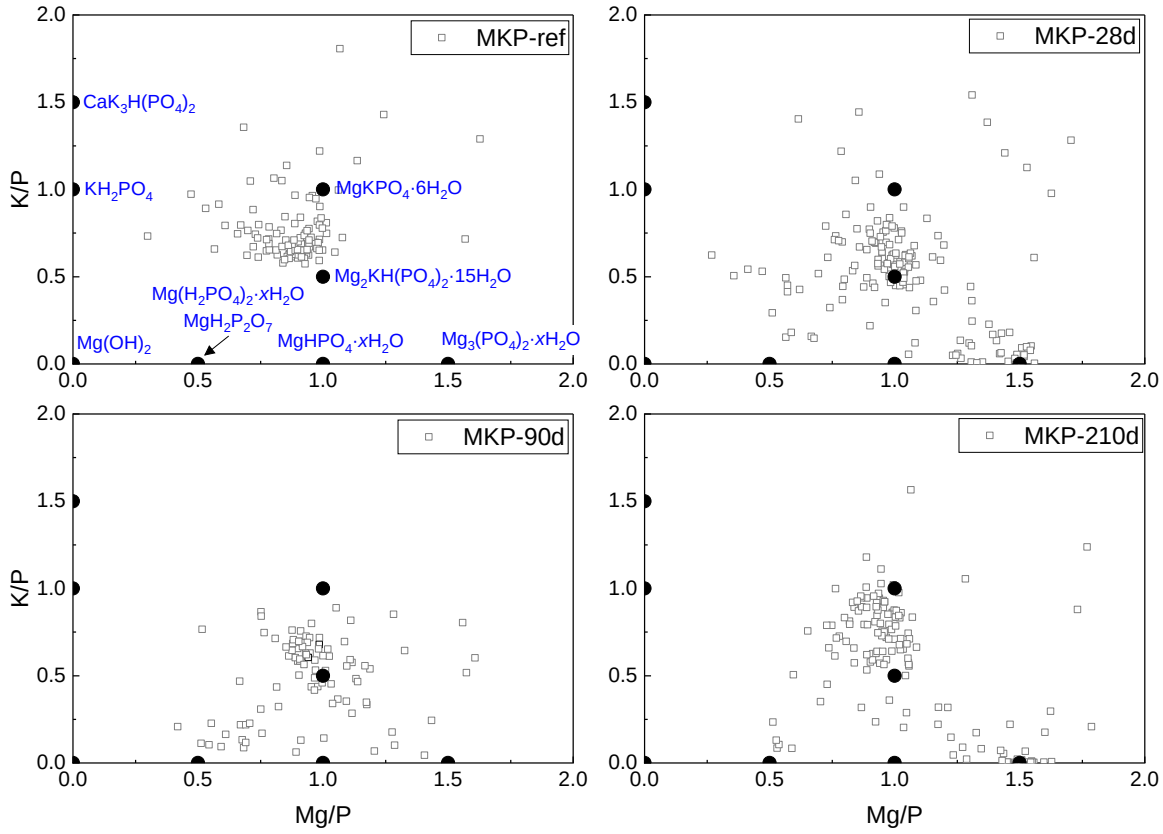

Figure 23 – *EDS mixing diagrams of K/P vs Mg/P atomic ratios determined on polished cross-sections of* ***(a)*** *MKP-ref (pristine cement paste), and leached solids:* ***(b)*** *MKP-28d,* ***(c)*** *MKP-90d, and* ***(d)*** *MKP-210d.*

The population of EDS points with K/P and Mg/P ratios close to those of K-struvite indicated that K-struvite was still present in the leached solids (zones 2 and 3, as evidenced by XRD). Furthermore, no dispersion of EDS points was observed towards residual KH_2PO_4, as noted before leaching. This indicates that residual KH_2PO_4 was fully exhausted and leached into solution.

Moreover, EDS data confirmed the precipitation of new phases with low K content. The Mg/P atomic ratio of these phases ranged from 0.5 to 1.5, corresponding to cattiite ($Mg_3(PO_4)_2{\cdot}22H_2O$), but also, possibly, to other phases with lower Mg/P atomic ratios such as newberyite or magnesium hydrogen phosphates ($Mg(H_2PO_4)_2{\cdot}xH_2O$, $MgH_2P_2O_7$,…). However, these phases were not evidenced by XRD, nor by ^{31}P MAS-NMR (results not shown).

4.2.2.4 Modeling the leaching of MKPC paste samples at pH 7

For modeling, the composition of the cement paste was simplified. The solid fraction was assumed to contain K-struvite, residual KH_2PO_4, MgO, as well as fly ash, but MgO and fly ash were considered as non-reactive. The composition of the pore solution was established using data acquired from experimental extractions of the pore solution ([K] = 1033.8 mmol/L, [P] = 370 mmol/L, [B] = 136.4 mmol/L and [Mg] = 1.1 mmol/L, pH = 8.0). Note that this solution was still oversaturated with respect to K-struvite (saturation index of 0.87 > 0). The initial porosity of the matrix was set at 15.5%, as determined experimentally, and the pore network was considered as fully saturated. To reproduce the leached cumulative concentrations of magnesium determined experimentally, the effective diffusion coefficient (D_e) was adjusted to 1.7×10^{-11} $m^2{\cdot}s^{-1}$. The parameters used to define the MKPC composition in the model are presented in Table 14.

***Table 14**. Parameters used to define the initial composition of the MKPC paste in the model. Concentrations are given in mmol/L of interstitial solution.*

	$MgKPO_4 \cdot 6H_2O$	KH_2PO_4	$B(OH)_3$	K_2O	Na_2O*	pH
mmol/L	20700	565	135	237	50	8.0

**Na_2O was added to adjust the pH at 8.0. Na_2O and K_2O are fictive species which fully dissolve, thus providing Na^+, K^+ and OH^- ions to the pore solution.*

The results obtained by modeling are presented in Figure 19. The model successfully reproduced the experimental trends for the leached cumulative concentrations of K and P, although the calculated concentrations were slightly underestimated. These underestimations may be attributed to the simplified composition considered for the cement paste, which neglected the contribution of impurities, fly ash, residual KH_2PO_4 and other phosphate phases that may be present in the solid (e.g., in the amorphous phase). Figure 19-d shows a discrepancy between experimental and modelled B concentrations. Experimentally, B was gradually released from the matrix and it was only depleted at the end of the 210-day leaching experiment. In contrast, the model predicted a much faster exhaustion of B, in 39 days only. Again, the bias in the model likely resulted from oversimplification of the paste composition. Boron was indeed added as soluble boric acid whereas experimental characterizations have shown that B partly precipitated as borophosphate phases of lower solubility [33].

Figure 24 displays the evolution of the paste composition calculated by modeling at 0, 28, 90 and 210 days of leaching. The values of effective diffusion coefficient (D_e) are displayed in a Y-axis logarithmic scale.

The model predicted an interface retreat of the leached solid, which increased with the leaching time (Figure 24-a, d, g, and j), as observed experimentally. At 210 days, the calculated retreat reached 1.15 mm, which was consistent with the experimental determination given the experimental uncertainty (1.0±0.2 mm, see Figure 20).

The model also reproduced fairly well the phase evolution, with dissolution of K-struvite and precipitation of cattiite, providing that formation of bobierrite ($Mg_3(PO_4)_2 \cdot 8H_2O$) and magnesium orthophosphate tetrahydrate ($Mg_3(PO_4)_2.4H_2O$) was excluded. These two minerals are more stable than cattiite from a thermodynamical point of view [10]. However, they were not detected experimentally in the solid, suggesting that their formation was kinetically hindered at room temperature. Modeling predicted a pH increase in the leached solid, which was confirmed experimentally by spraying the Rainbow indicator on a cross-section of the leached samples (Figure 20). In the simulation, the rise in pH could result from the fast depletion of borate ions, which contribute to buffer the pH in the range 8-9, and from the conversion of K-struvite into cattiite, releasing basic PO_4^{3-} anions (Eq. 7).

$$3(MgKPO_4 \cdot 6H_2O) + 4H_2O \rightarrow Mg_3(PO_4)_2 \cdot 22H_2O + PO_4^{3-} + 3K^+ \quad \text{(Eq. 7)}$$

When the pH reached 10.5, the model predicted the precipitation of brucite in the solid. This zone of brucite precipitation was narrower than that of cattiite, as the pH rapidly decreased to 7 at the interface, falling outside the stability domain of brucite. Destabilization of brucite was accompanied by transient reprecipitation of cattiite. The brucite precipitation predicted by the model was however not evidenced experimentally. Additional characterization of the leached samples (not shown here) were performed using thermogravimetry analysis. No weight loss was observed in the 350-400°C temperature range characteristic of brucite decomposition into periclase. Speciation of Mg in the

leached samples would deserve deeper investigation. Finally, the strong increase in porosity and effective diffusion coefficient was associated with the dissolution of K-struvite, despite the transient precipitation of cattiite. This increase in porosity may explain the very fragile nature of the external layer of the leached samples.

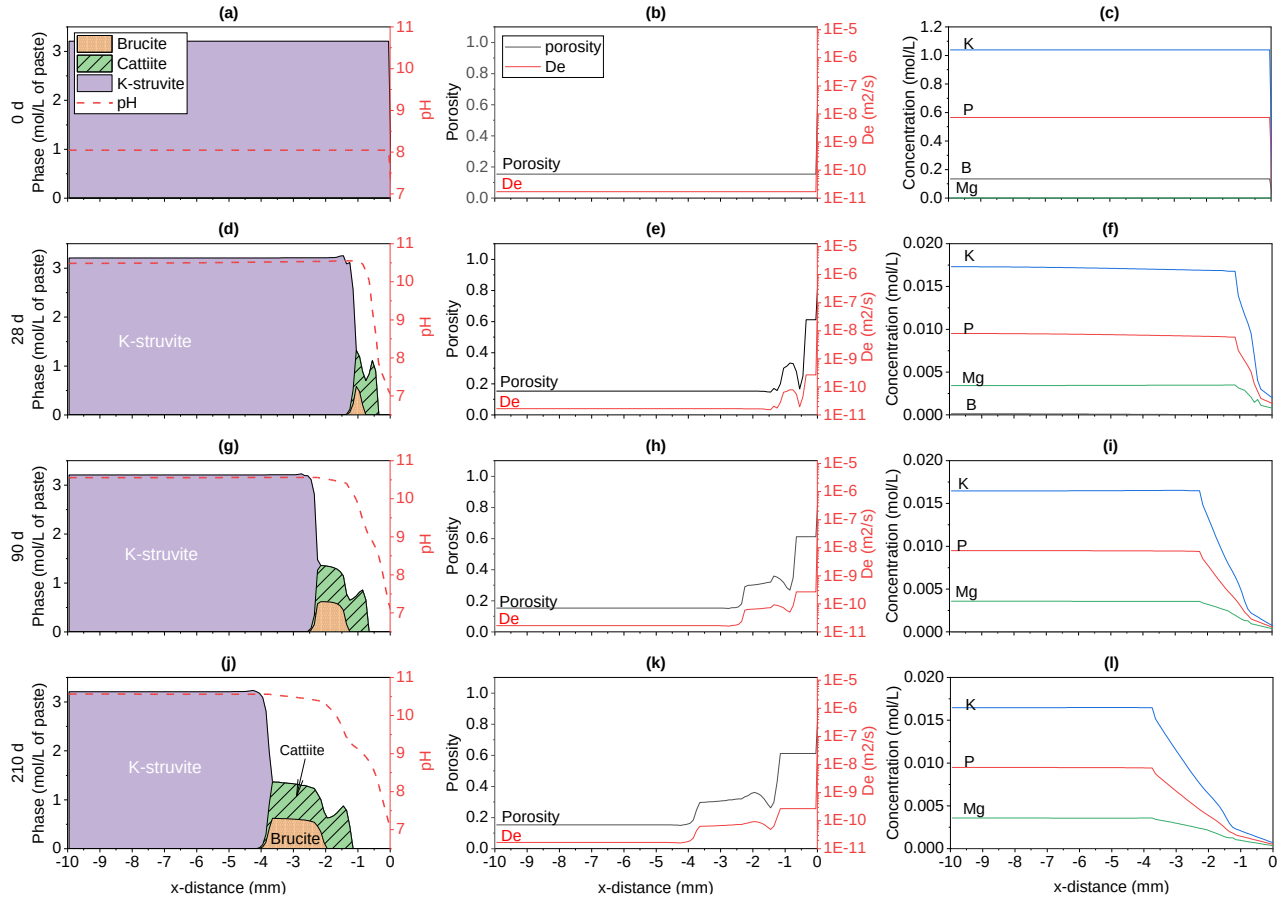

Figure 24 – *Predicted evolution of the paste composition at different stages of leaching,* ***(left)*** *mineral concentration and pH,* ***(middle)*** *porosity and effective diffusion coefficient (D_e),* ***(right)*** *B, K, P and Mg concentrations.*

4.2.3 Leaching of MKPC paste samples by an alkaline solution (pH 13.2)

4.2.3.1 Precipitates formed in the leachates

The leaching solution became turbid upon immersion of paste samples, indicating the formation of a precipitate in solution (Figure 25-a). Subsequently, after each renewal, solid and liquid phases were separated through centrifugation to isolate any precipitate that might have formed since filtration of solution using 0.2 µm membranes was insufficient. During the first two renewals, the precipitate was easily recovered. From the third renewal onwards, the clarity of the leaching solutions increased over time. The recovered precipitate was rinsed with ethanol and dried at 38 °C for 24 h. Its analysis by XRD revealed the formation of hydroxyapatite (HAP) (Figure 25-a).

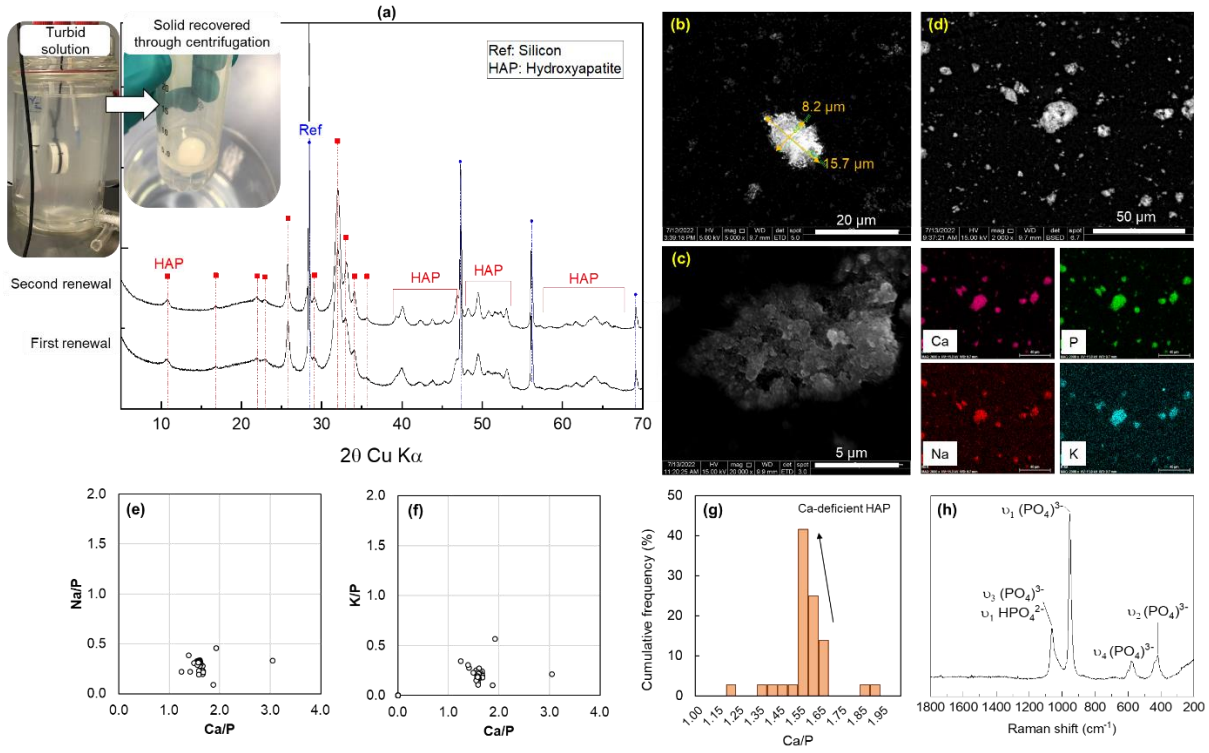

Figure 25 *– Characterization of HAP:* ***(a)*** *XRD patterns,* ***(b)*** *SE image,* ***(c)*** *zoomed-in of a single HAP particle,* ***(d)*** *BSE image and EDS elemental mapping, EDS semi-quantitative analyses : Na/P vs. Ca/P* ***(e)*** *and K/P vs. Ca/P atomic ratios* ***(f)****,* ***(g)*** *distribution of Ca/P atomic ratios, and* ***(h)*** *Raman spectrum.*

HAP particles consisted of agglomerates of micrometer-sized crystals (Figure 25-b and c). EDS analyses showed the presence of Ca, P, Na and K in the HAP particles, which suggested the uptake of alkalis by HAP, as already observed [39] (Figure 25-d, e and f). The distribution of Ca/P atomic ratios in the HAP particles exhibited a main mode at 1.59±0.11 (Figure 25-g). This atomic ratio suggested the precipitation of Ca-deficient HAP (CDHA), as stoichiometric HAP typically presents a Ca/P atomic ratio of 1.67.

Figure 25-h presents the Raman spectrum of the CDHA particles. The spectrum exhibited distinct bands, including the symmetric stretching mode (ν_1) of phosphate at approximately 962 cm^{-1}, which corresponds to the tetrahedral $(PO_4)^{3-}$ group (P−O bond) typically reported in HAP [40, 41]. The ν_4 and ν_2 bending modes (O−P−O bond) produced bands of weak intensity in the regions of 570–625 cm^{-1} and 400–490 cm^{-1}, respectively. The band at 1000-1095 cm^{-1} could be assigned to the ν_3 $(PO_4)^{3-}$ domain [40], but also to the ν_1 mode of hydrogen phosphate (HPO_4^{2-}) present in CDHA [41, 42].

4.2.3.2 Evolution of leached species in solution

Figure 26 shows the evolution of the cumulative concentrations of K, Na, Ca, P, B, Si, S and Al in the leachates and of the pH as a function of the square root of time. The Mg concentration always remained below the detection limit of the ICP-AES method (10 ppb). The red envelope represents the analytical error. The subfigure in Figure 26-c plots the difference between the Ca concentration measured in the leachates and the initial concentration in the leaching solution, which represents the Ca concentration consumed from the initial solution. Table 15 presents the initial composition of MKP-ref alongside with the cumulative leached element concentrations determined for each leaching period, expressed in mmol/g of paste. The leached fraction is presented as a percentage

for each element. The calculations were performed using an experimental density value of 1,876.2 kg/m^3.

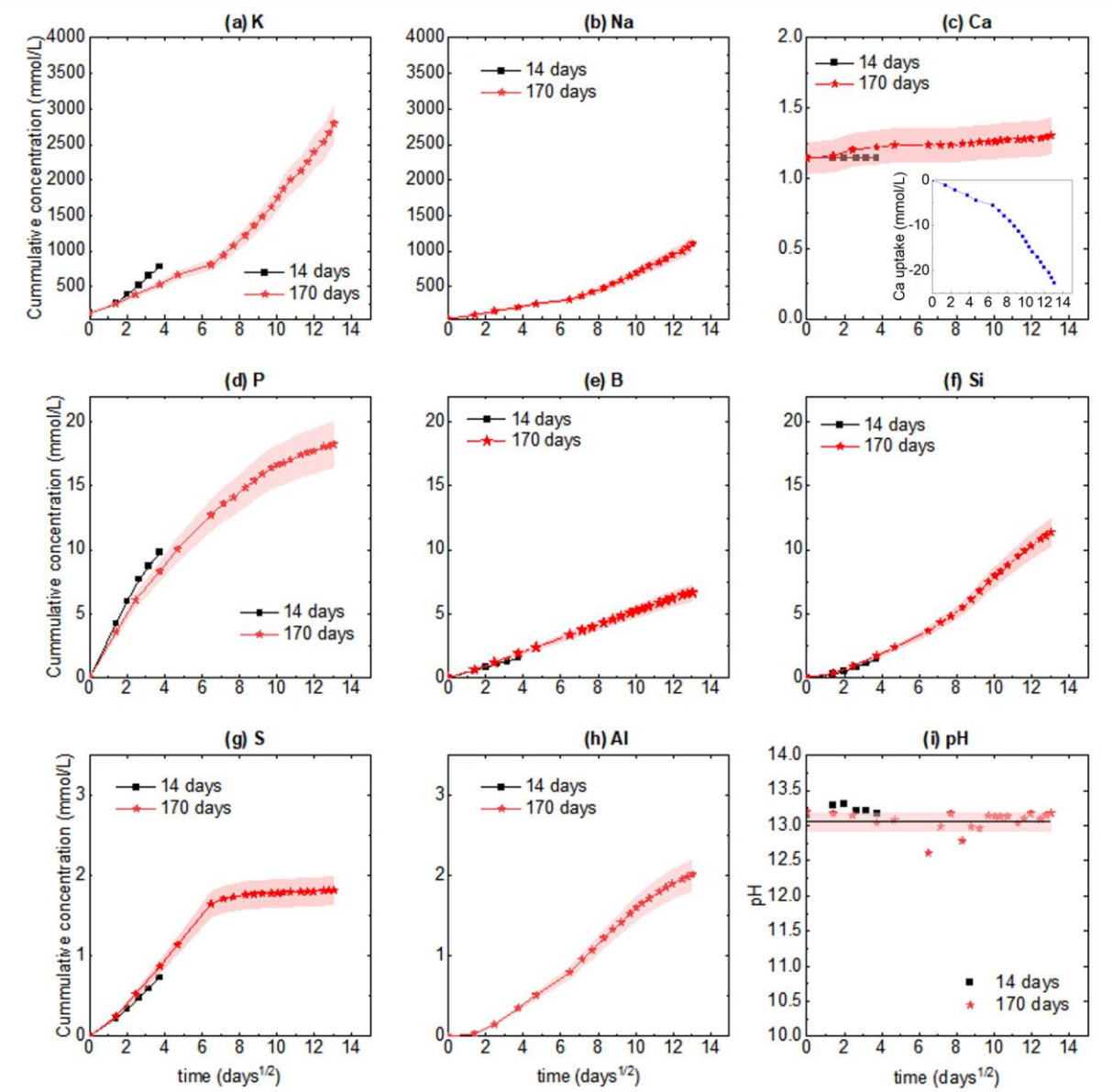

Figure 26. *Cumulative concentrations (in mmol/L) measured in the leachates as a function of the square root of time (days$^{1/2}$).* ***(a)*** *K,* ***(b)*** *Na,* ***(c)*** *Ca,* ***(d)*** *P,* ***(e)*** *B,* ***(f)*** *Si,* ***(g)*** *S,* ***(h)*** *Al, and* ***(i)*** *pH evolution. The analytical error is estimated to be 10 %.*

Table 15*. Initial and leached elemental concentrations (given in mmol/g of MKPC paste).*

			K	Na	Ca	Al	B	Fe	Mg	P	S	Si
	days	Initial concentration	2.8	0.1	0.3	1.9	0.13	0.6	2.4	2.6	0.04	3.8
Leaching time	14	Leached concentration	-	-	-	0.01	0.03	<ld	<ld	0.2	0.02	0.03
		Leached fraction (%)	-	-	-	0.33	26.5	0.0	0.0	8.7	40.1	0.87
	170	Leached concentration	-	-	-	0.0	0.13	<ld	<ld	0.4	0.04	0.26
		Leached fraction (%)	-	-	-	2.4	100	0.0	0.0	16.3	100	6.91

K and Na leached concentrations are not presented as their quantification fell into the 10% error associated with the ICP-AES technique. Fe and Mg concentrations were below the detection limit (d.l. = 10 ppb).

The two leaching experiments provided rather well repeatable results. Soluble phosphates (not including P precipitated as CDHA) were released in the leachates, but at a rate which decreased with time. The cumulative concentration of B in the leachates increased linearly versus the square root of time, suggesting that its release was controlled by diffusion through the pore network of the cement paste. Mass balance calculations in Table 15 show that B was depleted from the solid at the end of the 170-day leaching test. The leached Si, S, and Al resulted from dissolution of fly ash and/or impurities present in the raw materials. Si and Al cumulative concentrations exhibited similar evolution with time, while S was fully depleted after approximately 36 days of leaching. Unlike the other elements, calcium was significantly depleted from the leaching solution due to the precipitation of CDHA evidenced in section 4.2.3.1. Finally, it should be noted that the Mg concentration always remained below the detection limit of the ICP-AES method, which is a marked difference compared to the leaching test at pH 7.

4.2.3.3 Characterization of leached solids

Hereafter, MKPC paste samples recovered after 14 and 170 days of leaching will be referred to as MKP-14d and MKP-170d, respectively.

After leaching, paste samples presented thin white layers coating their exposed surfaces (Figure 27). The thickness of each sample was measured using a digital caliper. No interface retreat nor expansion was observed. The exposed surfaces of the leached solids exhibited pronounced brittleness, and material deposited on these surfaces could be easily removed, especially after 170 days of leaching. The Rainbow indicator was sprayed onto the cross-sections of the leached pastes. The colour transformation from greenish to purple-blue indicated a rise in pH from 8, before leaching, to a value higher than 10.

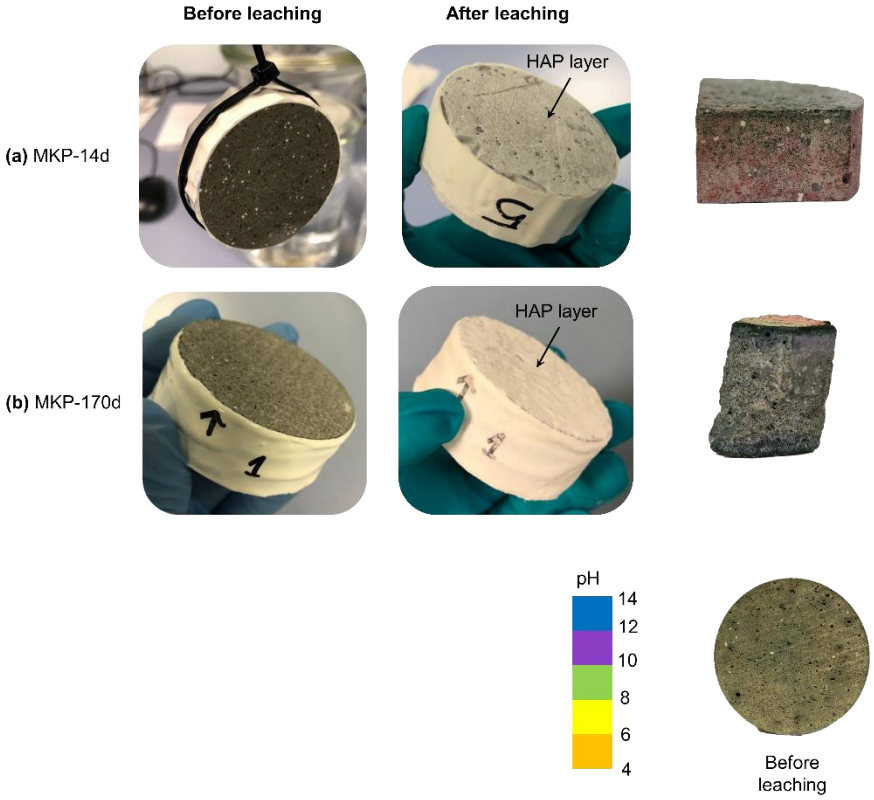

Figure 27. *Leached solids and estimation of pH using the Rainbow indicator:* ***(a)*** *MKP-14d, and* ***(b)*** *MKP-170d.*

4.2.3.3.1 SEM/EDS analyses

The layer observed on the exposed surface of the leached samples consisted of HAP. It measured approximately 12 ± 2 µm and 309 ± 38 µm in MKP-14d and MKP-170d, respectively (Figure 28-a and b) and was very porous. Under this superficial layer, a degraded zone was evidenced by a darker grey color on the SEM/BSE images, indicating a smaller density than that of the sound material. EDS elemental mapping showed some areas enriched in magnesium, suggesting the precipitation of a phase containing Mg, which could explain why Mg was not leached out of the sample (Figure 28 and Table 15). The elemental maps also showed a decrease in the P and K concentrations, which was consistent with the observed release of these species in the leachates.

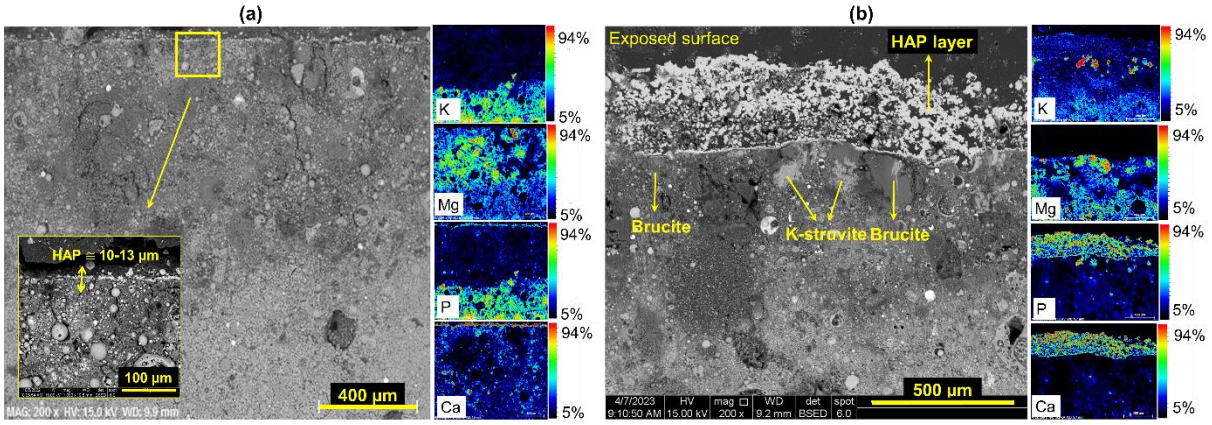

Figure 28. *SEM/EDS characterization of leached solids:* ***(a)*** *MKP-14d, and* ***(b)*** *MKP-170d.*

Figure 29 presents the mixing diagrams of atomic ratios based on EDS analyses and shows the regions corresponding to various phases potentially present in the solids, including residual KH_2PO_4, K-struvite, $Mg_2KH(PO_4)_2{\cdot}15H_2O$, bobierrite ($Mg_3(PO4)_2{\cdot}8H_2O$), cattiite ($Mg_3(PO4)_2{\cdot}22H_2O$), phosphorrösslerite ($MgHPO_4{\cdot}7H_2O$), newberyite ($MgHPO_4{\cdot}3H_2O$), brucite ($Mg(OH)_2$), hydroxyapatite ($Ca_5(PO_4)_3(OH)$), and $CaK_3H(PO_4)_2$ [10, 33]. Some additional phases were also included, such as magnesium hydrogen phosphate ($Mg(H_2PO_4)_2{\cdot}xH_2O$ or $MgH_2P_2O_7$), calcium silicate hydrate (C-S-H), and magnesium silicate hydrate (M-S-H) [10, 33, 43, 44]. After leaching, EDS point analyses were primarily carried out from the surface to a depth of 2 mm.

The P/Mg and K/Mg ratios measured in the leached samples tended to decrease as compared to the pristine material, suggesting the dissolution of K struvite, and the possible precipitation of brucite. In MKP-14d sample, the P/Mg and K/Mg ratios were still comprised between those of K-struvite and $Mg_2KH(PO_4)_2{\cdot}15H_2O$ for a number of point analyses, indicating the persistence of K-struvite after leaching (Figure 29-a). In MKP-170d sample, the scatter plot was shifted towards origin, suggesting advanced dissolution of K-struvite and higher precipitation of brucite. The mixing diagrams plotting the K/P vs. Ca/P ratios (Figure 29-b) showed the precipitation of a Ca-phosphate phase with a Ca/P ratio close to 1.5, such as CDHA, possibly intermixed, at the submicronic level, with other phases having lower Ca/P ratio, such as $CaK_3H(PO_4)_2$. Additionally, both leached solids presented EDS points with Mg/Si atomic ratios ranging from 0.7 to 1.4, which may correspond to the formation of Mg-silicates phases such as M_x-S-H_y, sepiolite ($Mg_4Si_6O_{15}(OH)_{12}{\cdot}6H_2O$), or chrysotile ($Mg_3(Si_2O_5)(OH)_4$) (Figure 29-c). No EDS points were related to the formation of C-S-H.

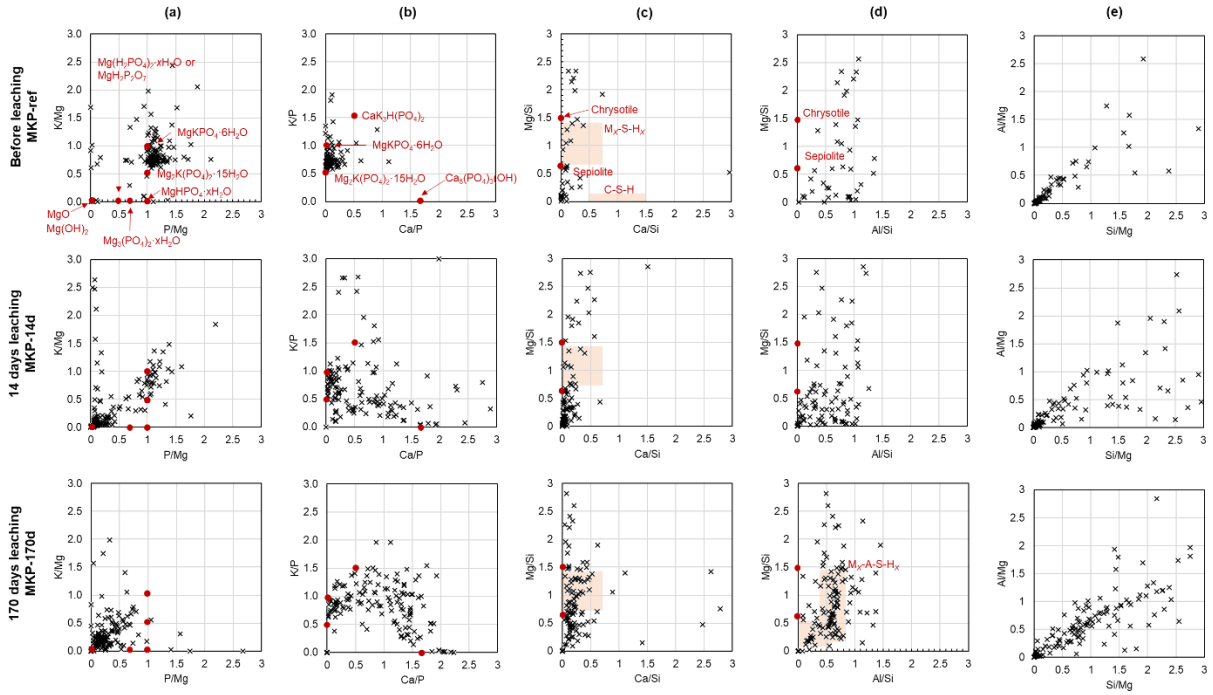

Figure 29. *EDS mixing diagrams of atomic ratios obtained from the MKPC paste samples before and after leaching:* ***(a)*** *K/Mg vs P/Mg,* ***(b)*** *K/P vs Ca/P,* ***(c)*** *Mg/Si vs Ca/Si,* ***(d)*** *Mg/Si vs Al/Si, and* ***(e)*** *Al/Mg vs Si/Mg.*

In MKP-170d, some EDS point analyses indicated the formation of a compound with Al/Si atomic ratios varying from 0.2 to 0.6, suggesting the presence of Al in Mg-silicate phases (Figure 29-d). The incorporation of aluminum in both tetrahedral and octahedral sites of M-S-H phases having a Mg/Si ratio of 1.1 or 1.7 has been evidenced by Bernard *et al.* [45]. Nevertheless, the Al/Si ratio was limited to 0.15−0.18. Another possible explanation would be the intermixing of magnesium silicate phases with hydrotalcite-like phases, Al-phosphates (such as minyulite ($KAl_2(PO_4)_2OH{\cdot}4H_2O$) or amorphous Al-phosphates) which have been predicted to form during hydration of MKPC materials containing aluminates [46], or mullite ($Al_{4+2x}Si_{2-2x}O_{10-x}$, possibly containing up to 0.5 wt% MgO [47]) supplied by the fly ash.

Finally, the Al/Mg *vs*. Si/Mg mixing diagram evidenced a correlation between the Al and Si contents for a number of analysis points (Figure 29-e), likely corresponding to the glassy fraction of fly ash [48]. The Al/Si ratios in the pristine material and in the paste leached for 14 days were close to 1. Interestingly, this value decreased to about 0.67 in the sample leached for 170 days, suggesting that non-congruent dissolution of the glassy phase(s) occurred during the longer leaching test, with preferential release of Al compared to Si. It has already been reported that when fly ash is exposed to a strongly alkaline solution, Al is more prone to dissolve than Si due to weaker Al-O bonds than Si-O bonds [49].

4.2.3.3.2 XRD analyses

Figure 30 displays some XRD patterns of powders obtained at different depths in MKP-14d and MKP-170d samples. The selected patterns are presented in the 5°-40° 2θ range to highlight the main differences. The crystalline phases and amorphous fraction in MKP-14d and MKP-170d samples were also quantified by Rietveld refinement.

K-struvite was detected in all the patterns of MKP-14d but was absent from the first layer (Δ1: 0-579 µm) of MKP-170d (Figure 30-b). Its content in the deepest investigated layer of MKP-14d was close to that of the pristine material. However, it was significantly higher in MKP-170d (72.8 wt% *vs*. 53.8

wt% in the pristine cement paste), indicating a progress of cement hydration during the leaching test, with the conversion of amorphous precursors into more crystalline K-struvite.

Leaching caused the precipitation of novel crystalline phases. XRD confirmed the precipitation of hydroxyapatite (Figure 30-a) with low crystallinity (broad peak at 10°-12° 2θ) near the exposed surface of the leached cement pastes, but also deeper in the materials. In MKP-170d, this peak seemed to shift towards higher angles, possibly due to the presence of meixnerite ($Mg_6Al_2(OH)_{18}\cdot 4H_2O$), which was identified up to a depth of 4.5 mm. Meixnerite is a Mg-Al layered double hydroxide (LDH) phase [47]. Among the different minerals tested containing Mg, Al and Si, it was the only one that provided acceptable refinement of the XRD patterns. Its amount varied between 1.4 wt% (0-579 µm layer) to 13.1 w% (1607-1919 µm layer). Moreover, brucite ($Mg(OH)_2$) precipitated in both leached solids, up to a depth of about 1 mm in MKP-14d, and 2.6 mm in MKP-170d. Finally, precipitation of low Ca/P calcium phosphates such as $CaK_3H(PO_4)_2$, hydrated magnesium silicate phases or alumino-phosphate phases such as OH-minyulite ($KAl_2(PO_4)_2OH\cdot 4H_2O$) was not evidenced by XRD.

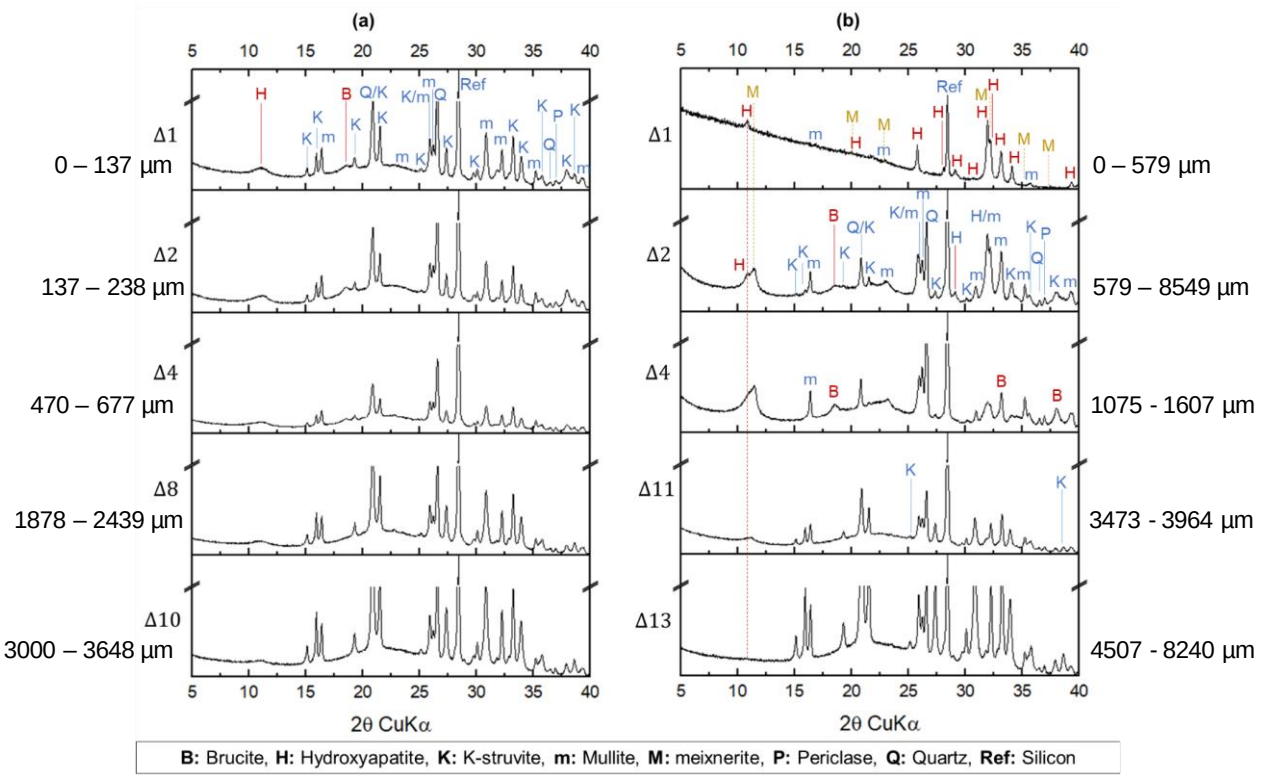

Figure 30. *XRD patterns obtained at different depths for* ***(a)*** *MKP-14d, and* ***(b)*** *MKP-170d.*

4.2.3.4 Modeling the leaching of MKPC paste samples under alkaline conditions

As for modeling of the leaching experiment at pH 7, the composition of MKPC paste was simplified (see 4.2.2.4 and Table 14). To reproduce the experimental precipitation front of brucite in the sample leached for 14 d, the effective diffusion coefficient (D_e) in the cement paste had to be adjusted at $1.37x10^{-13}$ m^2/s, which was significantly smaller than the diffusion coefficient used for the modeling at pH 7 (1.7×10^{-11} $m^2\cdot s^{-1}$) to reproduce the flux of Mg released in the leachate. This discrepancy still needs to be explained and underlines the need for an experimental determination of diffusion

coefficients in MKPC pastes. It also highlights the limits of the models tested (too simplified composition of leached solid, correlation between diffusion coefficient and porosity to be determined…).

Figure 31 displays the phase evolution, predicted by modeling, in the paste after 14 and 170 days of leaching. Dissolution of K-struvite occurred, producing an increase in porosity and effective diffusion coefficient. It was accompanied by the precipitation of brucite and hydroxyapatite (HAP) near the exposed surface, together with traces of hazenite. Note that precipitation of HAP was predicted to occur only close to the exposed surface, whereas it was experimentally observed deeper in the material and coexisted with brucite and K-struvite. The extent of K-struvite dissolution was well predicted in both pastes leached for 14 d and 170 d. Nonetheless, the thickness of the zone where brucite precipitated was underestimated by the model in MKP-170d. Moreover, the model predicted the gradual increase in pH from 8 in the sound core to 13 at the leached surface. HAP and brucite were also predicted to precipitate in the leaching solution. HAP precipitation in solution was in line with the experimental results. Nonetheless, brucite was not detected experimentally, possibly due to its low concentration. Besides, modeling tended to overestimate Ca concentrations and to underestimate P and B concentrations in solution.

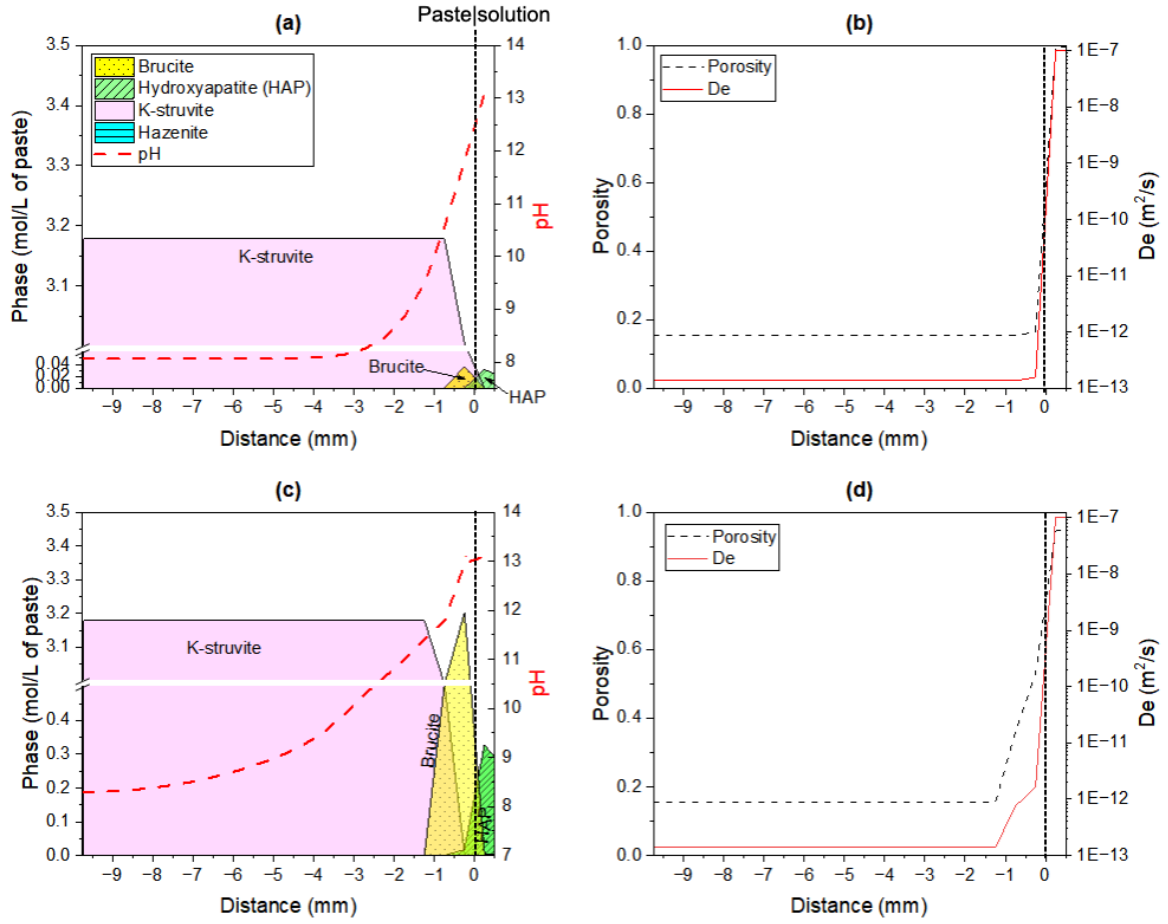

Figure 31. *Predicted evolution of the cement pastes: mineral phases and pH evolution, porosity, and effective diffusion coefficient (D_e) at (a), (b) 14 days, and (c), (d) 170 days of leaching. Traces of hazenite precipitated all along the paste (ranging from ≈2×10^{-11} to ≈1×10^{-4} mmol/L). Black dotted line indicates the paste-solution interface.*

Several hypotheses could be postulated to explain the differences between experimental and modeled results. *(i)* The paste composition was oversimplified in the model. *(ii)* The solubility of HAP

was overestimated. Thus, precipitation of HAP occurred only very close to the surface. It should be noted that there is a rather wide range of thermodynamic data reported for synthetic HAP [50], and thus, the extent of precipitation of HAP depends on the selected value.

Finally, the model predicted the precipitation of traces of hazenite ($Mg_2NaK(PO_4)_2.14H_2O$) in the leached solid. Hazenite concentrations were however too low (ranging from $2x10^{-11}$ to $1x10^{-4}$ mmol/L of paste) to be detected experimentally. Hazenite has been reported as a degradation product of K-struvite at pH >7 by several authors [11, 16], but is very difficult to evidence in cement pastes. Its crystal structure corresponds to a superstructure of K- and Na-struvite and thus possesses many structural features similar to those of K-struvite. Lahalle *et al.* [11] observed by SEM/EDS some sodium enrichment, and thus potentially the presence of hazenite, in cement pastes exposed to a synthetic PC pore solution. Xu *et al.* [16] succeeded in evidencing by XRD the precipitation of small amounts of hazenite when synthetic K-struvite was exposed to an alkaline solution, but failed to detect this phase when a cement paste was used.

4.3 Discussion

4.3.1 Leaching at pH 7: comparison between MKPC and Portland cement pastes

Degradation of MKPC and Portland cement pastes under leaching involves a combination of diffusive transport and chemical reactions. Diffusion of the dissolved species in the pore network appears as the rate-limiting step for both materials when leaching is performed at pH 7 under dynamic conditions. As a consequence, a zonation process is observed, involving dissolution/precipitation fronts. In MKPC paste, dissolution of K-struvite is accompanied by the transient precipitation of cattiite. In the Portland cement paste, the successive dissolution of portlandite, monosulfate (with transient reprecipitation of ettringite), ettringite and C-S-H phases is observed [51]. However, the extent of degradation at similar leaching times, is more important for MKPC sample than for a Portland cement paste (w/c = 0.4) having initially a slightly higher porosity accessible to water (c.a. 25 vol.%). After 90 days of leaching, the degradation front reaches 3.6 mm (including an interface retreat of 0.7 mm) for the MKPC paste, against 1.4 mm for the Portland cement paste [52]. The weaker resistance of the MKPC paste to leaching results from at least two factors: a higher diffusion coefficient, which may result from a higher fraction of macropores than in the Portland cement paste, and the presence of highly soluble phases (residual KH_2PO_4, impurities), which are readily leached out, thus increasing the total porosity and diffusion coefficient. To improve the durability of MKPC materials, two complementary approaches may be foreseen:

- Increase the Mg/P molar ratio of the cement to ensure total depletion of KH_2PO_4. An optimum should be found however to avoid the presence of excessive unreacted magnesia that raises the concern of brucite ($Mg(OH)_2$) formation in the long term and its possible detrimental influence on volume stability.
- Add a filler to modify the microstructure of the paste and thus, its transport properties. These properties are not only dependent on the total porosity but also on factors like the pore size distribution, tortuosity, and constrictivity within the cement matrix. As an example, a simulation carried out in this study shows that reducing the effective diffusion coefficient (D_e) from $1.7x10^{-11}$ m^2/s to $3x10^{-12}$ m^2/s, a value commonly used for modeling Portland cement-based materials with a water-to-cement (w/c) ratio of 0.5 [53], could limit the extent of degradation to 0.85 mm after 90 days of leaching.

4.3.2 Leaching of MKPC paste: influence of the leaching solution composition

In this work, two leaching solutions were used: *(i)* demineralized water with a pH set at 7, and *(ii)* an alkaline solution (pH 13.2 ± 0.1) mimicking the pore solution of conventional concrete prepared with CEM V cement (Portland cement blended with blast furnace slag and fly ash). In both cases, leaching induced mineralogical evolutions and a zonation process: K-struvite dissolved near the leached surface, and secondary phases precipitated, but their nature depended on the composition of the leaching solution.

- Under neutral conditions (pH 7), cattiite ($Mg_3(PO_4)_2.22H_2O$) precipitated in an intermediate zone, between the highly corroded superficial layer and the sound core.
- Under alkaline conditions (pH 13.2), hydroxyapatite precipitated on the external surface of the samples, whereas brucite, hydroxyapatite and Mg-silicate phases formed in an intermediate zone.

Leaching at pH 7 produced an interface retreat of the cement paste. On the contrary, with the alkaline leaching solution, no retreat nor expansion of the solid was evidenced. In this latter case, a layer of calcium-deficient hydroxyapatite, resulting from the reaction between Ca^{2+} ions present in the leaching solution and phosphate anions provided by the MKPC paste, formed at the solid/solution interface and its thickness increased with the leaching time (≈12 µm at 14 days, and ≈300 µm at 170 days). Even though hydroxyapatite (HAP) is a mineral known for its low solubility [42], its formation was not sufficient to ensure the long-term durability of MKPC pastes. The superficial layer was rather porous (as evidenced by SEM/EDS in Figure 28) and did not seem to play any protective role, since degradation continued to progress between 14 days and 170 days of leaching.

Another difference between the two leaching tests was the flux of magnesium released in the leachates. Under neutral conditions, the cumulative concentration of magnesium increased linearly with the square root of time, at a rate close to 1 $mmol.L^{-1}.d^{-1/2}$. Under alkaline conditions, the Mg concentration in the leachates always remained below 1 ppb, the detection limit of the ICP-AES method used. Magnesium dissolved from the cement phases almost entirely reprecipitated in the cement matrix. Two main phases formed: brucite, and an hydrotalcite-like phase, which may be meixnerite ($Mg_6Al_2(OH)_{18}.4H_2O$) according to its diffraction pattern (cf. Figure 30). Precipitation of this magnesium aluminate hydrate implied that the glassy fraction of fly ash partly dissolved, since it was the only source of aluminate in the system. Such reactivity of fly ash was also indicated by the decrease in its Al/Si content, as highlighted by EDS analyses (Figure 29). It was enhanced by the pH increase of the pore solution occurring in the leached sample. Modeling showed indeed a pH gradient from 8 (initial pH of the pore solution) to 13, and experimental observations using a pH indicator confirmed that the pH exceeded 10 in the leached solid (cf Figure 27). The mixing diagrams built from the EDS point analyses in the degraded part of the cement paste also suggested the precipitation of magnesium silicate phases, with Mg/Si atomic ratios ranging from 0.7 to 1.4, and possibly containing aluminate (Figure 29). These phases were not detected by XRD, which means that they were amorphous or poorly crystalline. Previous studies have also reported the presence of M-S-H upon hydration of MKP cement [43, 44]. M-S-H have an ill-defined layered structure similar to that of hydrated precursors of 2:1 and 1:1 phyllosilicates [54, 55, 56]. Their stoichiometry may vary, with a Mg/Si molar ratio typically comprised between 0.7 and 1.5 [55]. At Mg/Si ≈ 1.3, M-S-H coexist with brucite. They can also incorporate aluminum in their structure, in both tetrahedral and octahedral sites [45]. Nevertheless, they are stable for pH values comprised between 9 and 11 [55], which could limit their zone of occurrence in the leached samples. The poor crystallinity of M-(A)-S-H makes their characterization by XRD a difficult task [56]. It was attempted to highlight their presence by ^{29}Si MAS NMR. However, the collected spectra (not presented here) were complex due

to signals overlapping and did not enable to confirm or infirm M-(A)-S-H formation. Speciation of magnesium in the leached MKPC pastes would deserve more thorough investigation in a future study.

Finally, the alkaline solution appeared more aggressive than the solution at pH 7. Phase evolutions were observed until a depth of 4.5 mm from the exposed surface in the paste leached for 170 d at pH 13.2. As a comparison, mineralogical evolutions occurred until a depth of 4.1 mm – including the interface retreat - in the sample leached for 210 d at pH 7.

5 Conclusions and perspectives

The investigation carried out in the framework of WP4 task 6.3 focused on the leaching behaviour of magnesium potassium phosphate cement (MKPC) pastes using a “practical” approach, aiming at determining the leachability indices following ANSI ANS 16.1 standard, and a “comprehension” approach, aiming at understanding the degradation mechanisms. The main results are summarized hereafter.

- **“Operational” approach**

- Leaching tests were carried out on MKPC mortars in accordance with ANS 16.1standard, using blast furnace slag as a filler instead of, or together with fly ash in the MKPC reference formulation.
- Effective diffusion coefficients (D_e) and leachability indices (LI) were calculated from the cumulative concentrations of elements released in the leachates. When leaching was performed with distilled water, MKPC - BFS specimens led to the highest LI values for all elements (Mg, K, P). With an alkaline leaching solution, the highest LI values were also obtained with MKPC specimens containing blast furnace slag (MPC - FA - BFS and MPC - BFS) for all investigated elements, except K. In this latter case, using fly ash as a filler seemed more advantageous.
- For all tested materials, the major elements (K, Mg, P and B) showed limited leachability (LI≥9) in both distilled water and an alkaline solution mimicking the internal waters of radioactive waste storage facilities.
- The use of blast furnace slag as a filler, in principle, makes it possible to design a MKPC-based material with a chemical resistance at least as good as that obtained with fly ash.

- “**Comprehension” approach**

The leaching of MKPC paste samples was studied on paste monoliths using both demineralized water (pH maintained at 7 by automatic titration) and an alkaline solution mimicking the pore solution of a concrete prepared with CEM V cement (pH 13.2, $[Na^+]$ = 0.05 mol.L^{-1}, $[K^+]$ = 0.15 mol.L^{-1}, $[Ca^{2+}]$ = 0.001 mol.L^{-1}). The leaching solutions were periodically renewed and the leachates were analysed using ICP-AES. Post-mortem mineralogical characterizations (mainly by XRD and SEM-EDS) were also performed on the leached paste samples.

The main conclusions and prospects drawn from this study are as follows.

- Degradation of MKPC samples under leaching can be defined as a combination of diffusive transport and chemical reactions (dissolution/precipitation fronts), with diffusion as the rate limiting process, as evidenced by the linear evolution of cumulative leached element concentrations versus the square root of time.
- Degradation of MKPC paste samples increased continuously with the leaching time over the investigated period (210 d at pH 7, 170 d at pH 13.2).
- All leached samples showed a zonation process. In the leaching tests carried out under neutral conditions (pH 7), K-struvite was fully dissolved close to the exposed surface of the sample. Then, in an intermediate zone, K-struvite coexisted with cattiite. Deeper in the sample, cattiite was not detected anymore and the phase assemblage was close to that of the pristine material.

In the leaching tests conducted with the alkaline solution, Ca-deficient hydroxyapatite (CDHA) precipitated on the external surface of the samples. K-struvite dissolved near the exposed surface. In the intermediate zone, K-struvite coexisted with brucite, CDHA and an hydrotalcite-like phase (possibly meixnerite $Mg_6Al_2(OH)_{18}.4H_2O$). The additional formation of other phases such as M-(A)-S-H and hazenite was possible, but still needs to be confirmed.

- An interface retreat of the solid occurred when leaching was performed at pH 7. On the contrary, under alkaline conditions, a layer of CDHA rapidly formed on the exposed surfaces and its thickness increased with the leaching duration. However, it was not sufficient to clog the porosity and protect the samples from further degradation, as the alteration fronts were found deeper in the 170-day leached solid than in the 14-day leached solid.

- Based on these results, a first modeling approach using reactive transport was proposed and helped to gain insights into the degradation process of MKPC materials under leaching. Despite the simplified composition of the paste used for calculations, the model reproduced fairly well the main mineralogical changes observed experimentally (dissolution of K-struvite, precipitation of cattiite at pH 7, precipitation of brucite and hydroxyapatite at pH 13).

  - **Outlook**

- To improve modeling, future work should consider the determination of solubility products of boro-phosphate phases lacking in the literature to use a more realistic paste composition. Under alkaline leaching conditions, the glassy fraction of fly ash should be considered as reactive to enable the formation of phases containing aluminates and/or silicates. Finally, it would be necessary to measure experimentally the diffusion coefficient D_e in pristine and altered MKPC pastes to avoid adjusting this parameter in the model.

- Besides, the “comprehension” approach used in this study, combining experimentation under well-controlled conditions and modelling, should be extended to the investigation of MKPC pastes :

  - with Mg/P molar ratio higher than 1 to determine the influence of this parameter on their degradation process;

  - with blast furnace slag to determine how the change of filler modifies the degradation mechanisms of the material.

- Finally, since MKPC-based materials are potential candidates for the stabilization/solidification of waste containing aluminum metal, the magnitude of the pH increase induced by leaching should be evaluated more precisely, as well as its influence on the corrosion rate of Al metal. In the same way, it would be necessary to determine whether Al corrosion is influenced by the use of blast furnace slag as a filler, instead of fly ash.

6 Acknowledgements

A. Mesbah (CNRS, IRCELYON, France) and V. Montouillout (CNRS, CEMHTI, Orléans, France) are gratefully acknowledged their support concerning Rietveld refinements and MAS-NMR analyses.

7 Publication and conferences

Articles in peer-reviewed journals

- L. Diaz Caselles, C. Cau Dit Coumes, P. Antonucci, A. Rousselet, A. Mesbah, V. Montouillout, “Chemical degradation of magnesium potassium phosphate cement pastes during leaching by demineralized water: Experimental investigation and modelling”, Cem. Concr. Res. 178 (2024) 107456 doi: 10.1016/j.cemconres.2024.107456
- L. Diaz Caselles, C. Cau Dit Coumes, P. Antonucci, A. Rousselet, A. Mesbah, V. Montouillout, « Leaching of magnesium potassium phosphate cement pastes under alkaline conditions”, submitted to Applied Geochemistry
- S. Sayenko, V. Shkuropatenko, O. Pylypenko, H. Kholomieiev, S. Karsim, A. Zykova, “Production and properties of magnesium potassium phosphate cements containing ash and metallurgical slag additives for radioactive waste immobilization”, Nucl. Rad. Safety 2 (2023), pp 30-43 doi: 10.32918/nrs.2023.2(98).03

Presentations in conferences (including Deliverables and Milestones)

- L. Diaz Caselles, C. Cau Dit Coumes, P. Antonucci, A. Rousselet, A. Mesbah, “Leaching behavior of magnesium phosphate cements”. WP4: Innovations in metallic materials treatment and conditioning. PREDIS Workshop. April 2022 (Otaniemi, Espoo, Finlande).
- L. Diaz Caselles**,** C. Cau Dit Coumes, P. Antonucci, A. Rousselet, A. Mesbah, **“**Leaching behavior of magnesium phosphate cements”. 4th International Symposium on Cement-Based Materials for Nuclear Wastes - NUWCEM. May 2022 (Avignon, France).
- L. Diaz Caselles, C. Cau Dit Coumes, P. Antonucci, A. Rousselet, A. Mesbah, V. Montouillout. **“**Leaching behavior of magnesium phosphate cements”. Workshop: Processus et mécanismes aux interfaces solide/liquide/gaz : lixiviation, dissolution, corrosion, radiolyse, sorption, spéciation - GDR SciNEE. IMT Atlantique. July 2022 (Nantes, France).
- L. Diaz Caselles, C. Cau Dit Coumes, P. Antonucci, A. Rousselet, A. Mesbah, V. Montouillout. “Leaching behavior of magnesium phosphate cements”. WP4: Innovations in metallic materials treatment and conditioning. PREDIS Workshop. May 2023 (Mechelen, Belgium).
- L. Diaz Caselles, C. Cau Dit Coumes, P. Antonucci, A. Rousselet, A. Mesbah, V. Montouillout. **“**Understanding the behavior of magnesium potassium phosphate cements under leaching”. The 16th International Congress on the Chemistry of Cement 2023 (ICCC2023). “Further Reduction of CO_2 - Emissions and Circularity in the Cement and Concrete Industry” September 18–22, 2023 (Bangkok, Thailand).
- L. Diaz Caselles, C. Cau Dit Coumes, P. Antonucci, A. Rousselet, A. Mesbah, V. Montouillout, Understanding the behaviour of magnesium potassium phosphate cement pastes under leaching: experimental and modelling approaches, 6th International Workshop on Mechanisms and Modelling of Waste / Cement Interactions, Prague, Czech Republic, November 20-22 (2023)
- L. Diaz Caselles, G. Bon, C. Cau Dit Coumes, P. Antonucci, A. Rousselet, A. Mesbah, V. Montouillout, Leaching of magnesium phosphate cement pastes: influence of the Mg/P molar ratio, 12th ACI/RILEM International Conference on Cementitious Materials and Alternative Binders for Sustainable Concrete (ICCM 2024), Toulouse, France, June 23-26 (2024)
- C. Cau Dit Coumes, L. Diaz Caselles, G. Poras, A. Rousselet, A. Mesbah, V. Montouillout, Understanding the behaviour of magnesium potassium phosphate cements under alkaline environment, 2nd International Conference on Innovation in Low-Carbon Cement and Concrete Technology, London, UK, July 8-10 (2024)

8 References

[1] F. P. Glasser, “Progress in the immobilization of radioactive wastes in cement”, *Cem. Concr. Res.*, vol. 22, pp. 201–216, 1992, doi: 10.1016/0008-8846(92)90058-4.

[2] L. Ionascu, M. Nicu, C. Turcanu, F. Dragolici, and G. H. Rotarescu, “Study of the conditioning matrices for aluminium radioactive wastes”, *Rom. J. Phys.*, vol. 59, pp. 360–368, 2014.

[3] C. Cau Dit Coumes, D. Lambertin, H. Lahalle, P. Antonucci, C. Cannes, and S. Delpech, “Selection of a mineral binder with potentialities for the stabilization/solidification of aluminum metal”, *J. Nucl. Mater.*, vol. 453, pp. 31–40, 2014, doi: 10.1016/j.jnucmat.2014.06.032.

[4] B. Weill and J. Bradik, “US Patent n°4,756,762 - Magnesium phosphate cement systems”, 1988.

[5] A. S. Wagh, S.-Y. Jeong, and D. Singh, “High strength phosphate cement using industrial byproduct ashes”, *Proc. 1st Intern. Conf. on High Strength Concrete*, The American Society of Civil Engineers, pp. 542–553, 1997.

[6] A. S. Wagh, “Recent Progress in Chemically Bonded Phosphate Ceramics”, *ISRN Ceram.*, vol. 2013, pp. 1–20, 2013, doi: 10.1155/2013/983731.

[7] B. Xu, B. Lothenbach, A. Leemann, and F. Winnefeld, “Reaction mechanism of magnesium potassium phosphate cement with high magnesium-to-phosphate ratio”, *Cem. Concr. Res.*, vol. 108, pp. 140–151, 2018, doi: 10.1016/j.cemconres.2018.03.013.

[8] Z. Ding, B. Dong, F. Xing, N. Han, and Z. Li, “Cementing mechanism of potassium phosphate based magnesium phosphate cement”, *Ceram. Int.*, vol. 38, pp. 6281–6288, 2012, doi: 10.1016/j.ceramint.2012.04.083.

[9] B. Xu, F. Winnefeld, J. Kaufmann, and B. Lothenbach, “Influence of magnesium-to-phosphate ratio and water-to-cement ratio on hydration and properties of magnesium potassium phosphate cements”, *Cem. Concr. Res.*, vol. 123, p. 105781, 2019, doi: 10.1016/j.cemconres.2019.105781.

[10] B. Lothenbach, B. Xu, and F. Winnefeld, “Thermodynamic data for magnesium (potassium) phosphates”, *Appl. Geochemistry*, vol. 111, p. 104450, 2019, doi: 10.1016/j.apgeochem.2019.104450.

[11] H. Lahalle, C. Patapy, M. Glid, G. Renaudin, and M. Cyr, “Microstructural evolution/durability of magnesium phosphate cement paste over time in neutral and basic environments”, *Cem. Concr. Res.*, vol. 122, pp. 42–58, 2019, doi: 10.1016/j.cemconres.2019.04.011.

[12] Q. Yang, B. Zhu, and X. Wu, “Characteristics and durability test of magnesium phosphate cement-based material for rapid repair of concrete”, *Mater. Struct. Constr.*, vol. 33, pp. 229–234, 2000, doi: 10.1007/bf02479332.

[13] Y. Li and B. Chen, “Factors that affect the properties of magnesium phosphate cement”, *Constr. Build. Mater.*, vol. 47, pp. 977–983, Oct. 2013, doi: 10.1016/j.conbuildmat.2013.05.103.

[14] L. Chong, J. Yang, and C. Shi, “Effect of curing regime on water resistance of magnesium–potassium phosphate cement”, *Constr. Build. Mater.*, vol. 151, pp. 43–51, doi: 10.1016/j.conbuildmat.2017.06.056.

[15] M. Le Rouzic, T. Chaussadent, L. Stefan, and M. Saillio, “On the influence of Mg/P ratio on the properties and durability of magnesium potassium phosphate cement pastes”, *Cem. Concr. Res.*, vol. 96, pp. 27–41, 2017, doi: 10.1016/j.cemconres.2017.02.033.

[16] B. Xu, C. Cau Dit Coumes, D. Lambertin, and B. Lothenbach, “Compressive strength and hydrate assemblages of wollastonite-blended magnesium potassium phosphate cements exposed to different pH conditions”, *Cem. Concr. Compos.*, vol. 143, 2023, doi: 10.1016/j.cemconcomp.2023.105255.

[17] ANSI/ANS-16.1–2003 (R2017) “Measurement of the leachability of solidified low-level radioactive wastes by a short-term test procedure”, *American National Standards Institute*, Washington, DC, USA, 2017.

[18] L. J. Gardner, S. A. Bernal, S. A. Walling, C. L. Corkhill, J. L. Provis, and N. C. Hyatt, “Characterization of magnesium potassium phosphate cements blended with fly ash and ground granulated blast furnace slag”, *Cem. Concr. Res.*, vol. 74, pp. 78–87, Aug. 2015, doi: 10.1016/j.cemconres.2015.01.015.L.J.

[19] B. Xu, H. Ma, H. Shao, Z. Li, B. Lothenbach, “Influence of fly ash on compressive strength and micro-characteristics of magnesium potassium phosphate cement mortars,” *Cem. Concr. Res.*, vol. 99, pp 86–94 (2017), doi: 10.1016/j.cemconres.2017.05.008

[20] L. Chong, J. Yang and C. Shi, “Effect of curing regime on water resistance of magnesium–potassium phosphate cement,” *Constr. Build. Mater.*, vol. 151, pp 43-51 (2017), doi: 10.1016/j.conbuildmat.2017.06.056

[21] J. Torras, I. Buj, M. Rovira and J. de Pablo, “Semi-dynamic leaching tests of nickel containing wastes stabilized/solidified with magnesium potassium phosphate cements”, *J. Hazard. Mater.*, vol. 186, pp 1954-1960 (2011), doi:10.1016/j.jhazmat.2010.12.093

[22] U.S. Nuclear Regulatory Commission, Technical position on waste form, Washington D. C., 20555 Revision 1. Appendix A-7, 1991, https://www.nrc.gov/docs/ML0037/ML003752851.pdf

[23] S.Sayenko, V.Shkuropatenko, O.Pylypenko, H. Kholomieiev, S. Karsim and A.Zykova, “Production and properties of magnesium potassium phosphate cements containing ash and metallurgical slag additives for radioactive waste immobilization”, *Nuclear and Radiation Safety (Ukrainian journal),* vol. 2, pp 30-43 (2023), doi: 10.32918/nrs.2023.2(98).03

[24] R. Snellings *et al.*, “RILEM TC-238 SCM recommendation on hydration stoppage by solvent exchange for the study of hydrate assemblages”, *Mater. Struct. Constr.*, vol. 51, 2018, doi: 10.1617/s11527-018-1298-5.

[25] C. Frontera and J. Rodríguez-Carvajal, “FullProf as a new tool for flipping ratio analysis”, *Phys. B Condens. Mater*., 335, pp 219-222, 2003, doi:10.1016/S0921-4526(03)00241-2.

[26] D. Massiot *et al.*, “Modelling one- and two-dimensional solid-state NMR spectra”, *Magn. Reson. Chem.*, vol. 40, no. 1, pp. 70–76, 2002, doi: 10.1002/mrc.984.

[27] J. van der Lee, L. De Windt, V. Lagneau, and P. Goblet, “Module-oriented modeling of reactive transport with HYTEC”, *Comput. Geosci.*, vol. 29, pp. 265–275, 2003, doi: 10.1016/S0098-3004(03)00004-9.

[28] L. De Windt and R. Badreddine, “Modelling of long-term dynamic leaching tests applied to solidified/stabilised waste”, *Waste Manag.*, vol. 27, pp. 1638–1647, 2007, doi: 10.1016/j.wasman.2006.07.019.

[29] N. Neithalath, J. Weiss, and J. Olek, “Characterizing enhanced porosity concrete using electrical impedance to predict acoustic and hydraulic performance”, *Cem. Concr. Res.*, vol. 36, no. 11, pp. 2074–2085, 2006, doi: 10.1016/j.cemconres.2006.09.001.

[30] L. De Windt and P. Devillers, “Modeling the degradation of Portland cement pastes by biogenic organic acids”, *Cem. Concr. Res.*, vol. 40, pp. 1165–1174, 2010, doi: 10.1016/j.cemconres.2010.03.005.

[31] F. Adenot and M. Buil, “Modelling of the corrosion of the cement paste by deionized water”, *Cem. Concr. Res.*, vol. 22, pp. 489–496, 1992, doi: 10.1016/0008-8846(92)90092-A.

[32] W. Han, H. Chen, X. Li, and T. Zhang, “Thermodynamic modeling of magnesium ammonium phosphate cement and stability of its hydration products”, *Cem. Concr. Res.*, vol. 138, p. 106223, Dec. 2020, doi: 10.1016/j.cemconres.2020.106223.

[33] H. Lahalle, C. Cau Dit Coumes, C. Mercier, D. Lambertin , C. Cannes, S. Delpech and S. Gauffinet, “Influence of the w/c ratio on the hydration process of a magnesium phosphate cement and on its retardation by boric acid”, *Cem. Concr. Res.*, vol. 109, pp. 159–174, 2018, doi: 10.1016/j.cemconres.2018.04.010.

[34] I. K. Jeon, A. Qudoos, and H. G. Kim, “Influence of carbonation curing on hydration and microstructure of magnesium potassium phosphate cement concrete”, *J. Build. Eng.*, vol. 38, 2020, p. 102203, 2021, doi: 10.1016/j.jobe.2021.102203.

[35] A. Viani, G. Mali, and P. Mácová, “Investigation of amorphous and crystalline phosphates in magnesium phosphate ceramics with solid-state ^{1}H and ^{31}P NMR spectroscopy”, *Ceram. Int.*, vol. 43, pp. 6571–6579, Jun. 2017, doi: 10.1016/j.ceramint.2017.02.087.

[36] K. O. Kongshaug, H. Fjellvåg, and K. P. Lillerud, “The synthesis and crystal structure of a hydrated magnesium phosphate $Mg_3(PO_4)_2{\cdot}4H_2O$”, *Solid State Sci.*, vol. 3, pp. 353–359, 2001, doi: 10.1016/S1293-2558(00)01109-2.

[37] Á. Palomo, S. Alonso, A. Fernandez-Jiménez, I. Sobrados, and J. Sanz, “Alkaline activation of fly ashes: NMR study of the reaction products”, *J. Am. Ceram. Soc.*, vol. 87, pp. 1141–1145, 2004, doi: 10.1111/j.1551-2916.2004.01141.x.

[38] L. H. Merwin, A. Sebald, H. Rager, and H. Schneider, “^{29}Si and ^{27}Al MAS NMR spectroscopy of mullite”, *Phys. Chem. Miner.*, vol. 18, 1991, doi: 10.1007/BF00199043.

[39] W. R. Stoll and W. F. Neuman, “The uptake of sodium and potassium ions by hydrated hydroxyapatite”, *J. Am. Chem. Soc.*, vol. 78, pp. 1585–1588, 1956, doi: 10.1021/ja01589a022.

[40] G. Penel, G. Leroy, C. Rey, and E. Bres, “MicroRaman spectral study of the PO_4 and CO_3 vibrational modes in synthetic and biological apatites”, *Calcif. Tissue Int.*, vol. 63, pp. 475–481, 1998, doi: 10.1007/s002239900561.

[41] R. M. Wilson, J. C. Elliott, S. E. P. Dowker, and L. M. Rodriguez-Lorenzo, “Rietveld refinements and spectroscopic studies of the structure of Ca-deficient apatite”, *Biomater.*, vol. 26, pp. 1317–1327, 2005, doi: 10.1016/j.biomaterials.2004.04.038.

[42] J. C. Elliot, “Structure and Chemistry of the Apatites and Other Calcium Orthophosphates”, vol. 118, no. 12. Amsterdam, Elsevier, 1994. doi: 10.1021/ja945007t.

[43] B. Xu, F. Winnefeld, and B. Lothenbach, “Effect of temperature curing on properties and hydration of wollastonite blended magnesium potassium phosphate cements”, *Cem. Concr. Res.*, vol. 142, p. 106370, 2021, doi: 10.1016/j.cemconres.2021.106370.

[44] B. Xu, B. Lothenbach, and F. Winnefeld, “Influence of wollastonite on hydration and properties of magnesium potassium phosphate cements”, *Cem. Concr. Res.*, vol. 131, p. 106012, 2020, doi: 10.1016/j.cemconres.2020.106012.

[45] E. Bernard, B. Lothenbach, C. Cau Dit Coumes, I. Pochard, and D. Rentsch, “Aluminum incorporation into magnesium silicate hydrate (M-S-H)”, *Cem. Concr. Res.*, vol. 128, 2019, p. 105931, 2020, doi: 10.1016/j.cemconres.2019.105931.

[46] B. Xu, F. Winnefeld, B. Ma, D. Rentsch, and B. Lothenbach, “Influence of aluminum sulfate on properties and hydration of magnesium potassium phosphate cements” , *Cem. Concr. Res.*, vol. 156, p. 106788, 2022, doi: 10.1016/j.cemconres.2022.106788.

[47] S. Koritnig and P. Süsse, “Meixnerite, $Mg_6Al_2(OH)_{18}\cdot 4H_2O$, ein neues Magnesium-Aluminium-Hydroxid-Mineral”, *TMPM Tschermaks Mineral. und Petrogr. Mitteilungen*, vol. 22, pp. 79–87, 1975, doi: 10.1007/BF01081303.

[48] K.L. Aughenbaugh, P. Stutzman and M.C.G Juenger, “Identifying glass compositions in fly ash”, *Front. Mater.,* vol. 3, 2016, doi: 10.3389/fmats.2016.00001.

[49] C. Li, Y. Li, H. Sun and L. Li, “The composition of fly ash glass phase and its dissolution properties applying to geopolymeric materials”, *J. Amer. Ceram. Soc.*, vol. 94, 1773–1778, 2011, doi: 10.1111/j.1551-2916.2010.04337.x.

[50] P. Vieillard and Y. Tardy, “Thermochemical Properties of Phosphates”, in: “Phosphate Minerals”. Springer Berlin Heidelberg, pp. 171–198, 1984, doi: 10.1007/978-3-642-61736-2_4.

[51] P. Faucon, F. Adenot, J. Jacquinot, J. Petit, R. Cabrillac and M. Jorda, “Long-term behaviour of cement pastes used for nuclear waste disposal: review of physico-chemical mechanisms of water degradation”, *Cem. Concr. Res.*, vol. 28, pp 847–857, 1998, doi: 10.1016/S0008-8846(98)00053-2.

[52] F. Adenot, ”Durabilité du béton : caractérisation et modélisation des processus physiques et chimiques de dégradation du ciment”, PhD Thesis, Orléans University, 1992.

[53] S. Bejaoui and B. Bary, “Modeling of the link between microstructure and effective diffusivity of cement pastes using a simplified composite model”, *Cem. Concr. Res.,* vol. 37, pp 469-480, 2007; doi: 10.1016/j.cemconres.2006.06.004.

[54] E. Bernard, B. Lothenbach, C. Chlique, M. Wyrzykowski, A. Dauzères, I. Pochard and C. Cau Dit Coumes, “Characterization of magnesium silicate hydrate (M-S-H)”, *Cem. Concr. Res.*, vol. 116, pp 309–330, 2019, doi: 10.1016/j.cemconres.2018.09.007.

[55] D. Nied, D., K. Enemark-Rasmussen, E. L’Hopital, J. Skibsted and B. Lothenbach, “Properties of magnesium silicate hydrates (M-S-H)”, *Cem. Concr. Res.,* vol. 79, pp 323–332, 2016, doi: 10.1016/j.cemconres.2015.10.003

[56] C. Roosz, S. Grangeon, P. Blanc, V. Montouillout, B. Lothenbach, P. Henocq, E. Giffaut, P. Vieillard and S. Gaboreau, “Crystal structure of magnesium silicate hydrates (M-S-H): the relation with 2:1 Mg–Si phyllosilicates”, *Cem. Concr. Res.,* vol. 73, pp 228–237, 2015, doi: 1016/j.cemconres.2015.03.014